

Searching for the Imprints of AGN Feedback on the Lyman Alpha Forest Around Luminous Red Galaxies

Vikram Khaire,^{1,2} Teng Hu,² Joseph F. Hennawi,^{2,3} Joseph N. Burchett,⁴
Michael Walther^{5,6} and Frederick Davies^{2,7}

¹Indian Institute of Space Science & Technology, Thiruvananthapuram, Kerala 695547, India

²Physics Department, Broida Hall, University of California Santa Barbara, Santa Barbara, CA 93106-9530, USA

³Leiden Observatory, Leiden University, PO Box 9513, NL-2300 RA Leiden, the Netherlands

⁴Department of Astronomy, New Mexico State University, 1320 Frenger Mall, Las Cruces, NM 88003-8001, USA

⁵University Observatory, Faculty of Physics, Ludwig-Maximilians-Universität München, Scheinerstr. 1, 81677 München, Germany

⁶Excellence Cluster ORIGINS, Boltzmannstrasse 2, D-85748 Garching, Germany

⁷Max-Planck-Institut für Astronomie, Königstuhl 17, 69117 Heidelberg, Germany

16 November 2023

ABSTRACT

We explore the potential of using the low-redshift Lyman- α ($\text{Ly}\alpha$) forest surrounding luminous red galaxies (LRGs) as a tool to constrain active galactic nuclei (AGN) feedback models. Our analysis is based on snapshots from the Illustris and IllustrisTNG simulations at a redshift of $z = 0.1$. These simulations offer an ideal platform for studying the influence of AGN feedback on the gas surrounding galaxies, as they share the same initial conditions and underlying code but incorporate different feedback prescriptions. Both simulations show significant impacts of feedback on the temperature and density of the gas around massive halos. Following our previous work, we adjusted the UV background in both simulations to align with the observed number density of $\text{Ly}\alpha$ lines (dN/dz) in the intergalactic medium and study the $\text{Ly}\alpha$ forest around massive halos hosting LRGs, at impact parameters (r_{\perp}) ranging from 0.1 to 100 pMpc. Our findings reveal that dN/dz , as a function of r_{\perp} , is approximately 1.5 to 2 times higher in IllustrisTNG compared to Illustris up to r_{\perp} of ~ 10 pMpc. To further assess whether existing data can effectively discern these differences, we search for archival data containing spectra of background quasars probing foreground LRGs. Through a feasibility analysis based on this data, we demonstrate that $\text{dN}/\text{dz}(r_{\perp})$ measurements can distinguish between feedback models of IllustrisTNG and Illustris with a precision exceeding 12σ . This underscores the potential of $\text{dN}/\text{dz}(r_{\perp})$ measurements around LRGs as a valuable benchmark observation for discriminating between different feedback models.

Key words: Add these before submission

1 INTRODUCTION

The formation and evolution of galaxies remain some of the most intriguing enigmas in modern astrophysics. Among the key puzzles is the disparity between blue star-forming galaxies and red quiescent elliptical galaxies, the steep decline of cosmic star formation rate density at $z < 2$, as well as the suppression of luminous galaxies in massive dark matter halos. The underlying physics behind these phenomena and the mechanisms responsible for shaping the fate of galaxies are still open questions in the field of galaxy formation (see reviews by Naab & Ostriker 2017; Vogelsberger et al. 2020). Current cosmological simulations attempt to reproduce these observations by harnessing the power of central supermassive

black holes, by a mechanism generally referred to as Active Galactic Nuclei (AGN) feedback, which drives galactic-scale winds that stifle star formation in massive galaxies at late cosmic times. However, the exact manifestation of AGN feedback is hotly debated (see e.g. Springel 2005; Croton et al. 2006; Sijacki et al. 2007; Hopkins et al. 2008), and the diversity of modeling approaches in recent simulations (e.g. Dubois et al. 2014; Genel et al. 2014a; Schaye et al. 2015; Khandai et al. 2015; Bolton et al. 2017; Weinberger et al. 2017; Davé et al. 2019) are a testament to the limited understanding and observational constraints of this intricate physical process.

Cosmological simulations of galaxy formation adjust

their feedback parameters using various observations such as star formation rate density, stellar mass function, galaxy sizes and color distribution, and total gas fraction within a radius R_{500c} ¹ of halo (as done in IllustrisTNG; Weinberger et al. 2017). But there are no simulations that adjust the parameters using observations of gas around galaxies beyond R_{500c} and into the intergalactic medium (IGM). Because these AGN feedback driven powerful galactic-scale winds and outflows not only stifle star formation in galaxies but also influence the gas in the circumgalactic medium (CGM) and the IGM (Gurvich et al. 2017; Burkhart et al. 2022; Tillman et al. 2022; Mallik et al. 2023; Khaira et al. 2023), it would be important to investigate if the observations of CGM and IGM can be used to constrain the parameters of feedback.

With this objective in mind, in our recent work (Khaira et al. 2023, hereafter Paper I), we studied the IGM in Illustris (Genel et al. 2014a) and IllustrisTNG (Weinberger et al. 2017) simulations at $z < 0.3$. These simulations provide an ideal test-bed for studying the effect of AGN feedback on CGM and IGM. This is because both simulations share the same underlying code and similar cosmological parameters and the primary difference between them lies in their implementation of AGN feedback (see Pillepich et al. 2018a). Illustris uses a strong radio-mode thermal feedback and IllustrisTNG employs a milder kinetic radio-mode feedback. This difference in the feedback implementation leads to significant differences in the distribution of baryons around massive halos and in the IGM. In Paper I, we found that feedback can severely affect IGM and thereby affect various statistical measures used to study IGM. This is mainly because the fraction of cool baryons responsible for the Ly α forest itself is affected by the feedback. However, while comparing various IGM statistics with observations, one needs to adjust the UV background (see Haardt & Madau 2012; Khaira & Srianand 2019; Faucher-Giguère 2020) in simulations because the mean optical depth of the Ly α forest depends on the degenerate combination of the UV background and cool baryon fraction. After such adjustment most of the statistics of Ly α forest such as line density and 2D and marginalized distributions of Doppler widths (b) and H I column density (N_{HI}), do not show any significant difference between simulations. Only the Ly α flux power spectrum (as measured in Khaira et al. 2019) at small spatial scales exhibits potentially observable differences (refer to Paper I, for more details). Therefore it is important to investigate if there is any other statistic of IGM and CGM that can distinguish the effect of feedback.

Although the IGM's usefulness is somewhat limited due to its degeneracy with the UV background, notable distinctions in gas distribution around massive galaxy halos still persist (as illustrated in Fig. 1). This forms the core of our investigation in this paper. Here we study the gas around massive halos as probed by absorption spectra of the background quasar. We generate realistic Ly α forest spectra of background quasars probing the gas around massive halos in the foreground at different transverse distances (i.e impact parameter) from halos and study a few statistics such as

marginalized and 2D distribution of b and N_{HI} , and number density of lines as a function of impact parameter, dN/dz (r_{\perp}). We found that in realistic spectra where we forward model the Hubble Space Telescope (HST) Cosmic Origin Spectrograph (COS) data, the differences in the b - N_{HI} distribution wash out but the number of absorption lines vary dramatically in both simulations. This discrepancy manifests as a significant difference in dN/dz (r_{\perp}) values of Illustris and IllustrisTNG, extending up to an impact parameter of approximately $r_{\perp} \sim 10$ pMpc.

To investigate the utility of dN/dz (r_{\perp}) for distinguishing different feedback models as employed in Illustris and IllustrisTNG, we conducted a search for a catalog of quasar-galaxy pairs within the available HST-COS quasar spectra (Peeples et al. 2017), coupled with luminous red galaxies from the Sloan Digital Sky Survey (SDSS; York et al. 2000). This search yielded a dataset comprising 94 background quasars probing approximately 3193 foreground luminous red galaxies (LRGs) up to an impact parameter of ~ 10 pMpc. To gauge the potential of this dataset, we generated a simplified mock representation of these quasar-LRG pairs based on simulations. Our analysis reveals that if the actual feedback mechanisms resemble those presented in the IllustrisTNG simulation, then the observed dN/dz (r_{\perp}) values derived from these 3193 quasar-LRG pairs can effectively distinguish this scenario from the Illustris feedback model. The statistical significance of this distinction exceeds 12σ . This outcome underscores the potential of dN/dz (r_{\perp}) as a robust tool for constraining AGN feedback models. In our forthcoming work, we intend to take a step further by measuring dN/dz (r_{\perp}) from archival HST-COS data. This effort will shed light on which feedback models align with observed dN/dz (r_{\perp}), providing further insights into the complex interplay between AGN feedback and galaxy formation.

The paper is organized as follows. In Section 2, we provide an overview of the simulations used in this study. Section 3 outlines our methodology, including the selection of halos hosting LRGs, the generation of realistic Ly α forest spectra probing these galaxies, and our Voigt-profile fitting procedure. In Section 4, we present the results of our analysis, encompassing various statistical measures, and conduct a feasibility analysis regarding the use of dN/dz (r_{\perp}) statistics on archival HST-COS data. Finally, in Section 5 we summarise the results of the paper.

2 SIMULATIONS

Following Paper I, we use Illustris (Vogelsberger et al. 2014; Genel et al. 2014b) and the IllustrisTNG (Weinberger et al. 2017; Pillepich et al. 2018a) galaxy formation simulations to study the impact of AGN feedback on the gas around halos of galaxies. Because both simulations are run with the same initial condition, we identify the same dark matter halos in both to investigate the difference in gas distribution surrounding them. Both simulations are also run with the same underlying AREPO code (Springel 2010), but as compared to Illustris the ideal magnetohydrodynamic calculations were used for IllustrisTNG. These simulations incorporate an array of astrophysical processes needed for galaxy formation and modeling the Ly α forest. These include star formation Pillepich et al. (2018b), feedback from both stars and AGN, the influence of

¹ R_{500c} represents the radius of a sphere surrounding halos, encompassing a mass density that is 500 times the critical matter density.

Table 1. Cosmology parameters used in simulations

Parameters	Illustris	IllustrisTNG
Ω_m	0.2726	0.3089
Ω_Λ	0.7274	0.6911
Ω_b	0.0456	0.0486
h	0.704	0.6774
σ_8	0.809	0.8159
n_s	0.963	0.97

galactic winds (Nelson et al. 2019), the process of chemical enrichment (Naiman et al. 2018), photoionization heating using the UV background model of Faucher-Giguère et al. (2009), and various cooling mechanisms including metal cooling.

The main difference between Illustris and IllustrisTNG simulation is the feedback prescription. Illustris failed to reproduce a few critical observations such as the distribution of red and blue galaxies (Nelson et al. 2018), populations of discs among galaxies (Pillepich et al. 2019), and the gas mass fraction within R_{500c} of the halos. In order to alleviate these issues many of the feedback prescriptions were changed in the updated simulation; IllustrisTNG. For an in-depth account of these updates, we recommend a comprehensive summary outlined in Table 1 of Pillepich et al. (2018a).

The primary distinction in feedback prescription, which significantly impacts the gas surrounding massive galaxies and the IGM, lies in the implementation of radio mode AGN feedback. In the Illustris simulation, a bubble mode feedback approach was employed, where the energy released by central AGN was accumulated over time and then explosively released into the surrounding environment. This process generated large, hot gas bubbles around massive halos in Illustris and substantially reduced the gas content within the region of R_{500c} surrounding these halos. Conversely, IllustrisTNG utilized a kinetic radio mode feedback mechanism, wherein the energy released from central AGNs was used to drive the winds by imparting stochastic momentum kicks to nearby particles. These distinct approaches to AGN feedback are anticipated to influence the gas properties around massive galaxies, prompting our investigation into whether these properties can effectively serve as probes for the feedback mechanisms themselves.

Apart from the distinct AGN feedback prescriptions, there exists a slight variation in the cosmological parameters applied in both simulations, as outlined in Table 1. Although we anticipate that these minor differences in cosmological parameters would have an insignificant impact on the properties of gas within the IGM and CGM, we maintained the respective cosmological parameters in our analysis of the Ly α forest. This choice ensures a fair and consistent comparison between the two simulations.

It is expected to have a large impact of feedback at lower redshifts, therefore, as in Paper I, we choose a simulation snapshot at $z = 0.1$. We used publically available snapshots at $z = 0.1$ of both Illustris² and IllustrisTNG³ having a box size of 75 cMpc/h and 1820³ dark matter and baryon particles each. In order to study the gas around galaxies and then generate synthetic Ly α forest, we first convert the simula-

tion snapshots of both Illustris and IllustrisTNG into 3D Cartesian grids. This is achieved by depositing smoothed quantities such as density, temperature, and velocities from Voronoi mesh output of simulations onto 1820³ grids. For calculating smoothed quantities we follow the standard approach of using a Gaussian kernel with a radius equal to 2.5 times the radius of each Voronoi cell by assuming each Voronoi cell is spherical. As mentioned in Paper I, this way of fixing Gaussian kernel size and the choice of factor 2.5 is arbitrary but often used for Illustris and IllustrisTNG simulations (private communication with D. Nelson).

2.1 Gas Around the Same Halo: An illustration

Given the distinct radio-mode AGN feedback implementations in Illustris and IllustrisTNG, these simulations offer a valuable opportunity to explore the impact of AGN feedback on gas distribution around galaxy halos and within the IGM. Notably, since these simulations share identical initial conditions, enabling us to find the same halos for a direct comparison of differences in the distribution of gas around them. This is illustrated in Fig. 1. The figure shows a 2D slice of the hydrogen density and temperature profile around the same halo in both simulations. The slice has a thickness equal to one grid cell (i.e. of size ~ 60 ckpc). The halos were identified by matching the coordinates of halos in the halo catalogs provided by Illustris and IllustrisTNG. The dashed circles at the center of each panel have a radius equal to the virial radius of the halo. The density and temperature profiles shown in this example demonstrate that Illustris expels hot gas further from the central halo as compared to the IllustrisTNG (see density profile in left-hand panels), and also generates a huge > 10 pMpc size shock-heated hot region identified by the transition from shock heated $\sim 10^6$ K gas to 10^4 K photoionized gas (see right-hand panels). The size of the bubble in Illustris halo is up to the size of 20 virial radii ($R_{\text{vir}} = 0.57$ pMpc for $10^{13.1} M_\odot$ halo at $z = 0.1$). This expulsion of gas also leads to small differences in the masses of halos that are calculated by summing the mass of all particles and cells within R_{200c} , resulting in slightly less mass for the Illustris halo ($10^{13.1} M_\odot$) as compared to IllustrisTNG ($10^{13.2} M_\odot$). Fig. 1 shows that there are significant differences in the distribution of gas density and temperature around the same halos in both simulations. Only in some regions far away from halos, the density and temperature profiles are similar in both simulations (for e.g. notice a filament at the bottom left corner of Fig. 1).

The differences in gas temperature and density surrounding halos provide a compelling reason to explore statistical metrics that can effectively differentiate between the feedback disparities in both simulations. The subsequent section outlines our methodologies for examining the gas properties around massive halos within these simulations.

3 METHODS TO GENERATE SYNTHETIC LYMAN ALPHA FOREST AROUND MASSIVE HALOS

In this section, we describe the methodology employed for the selection of massive halos in both simulations, the generation of synthetic Ly α forest spectra in the IGM and in the vicinity of halos, the forward modeling approach applied

² Illustris: <https://www.illustris-project.org>

³ IllustrisTNG: <https://www.tng-project.org>

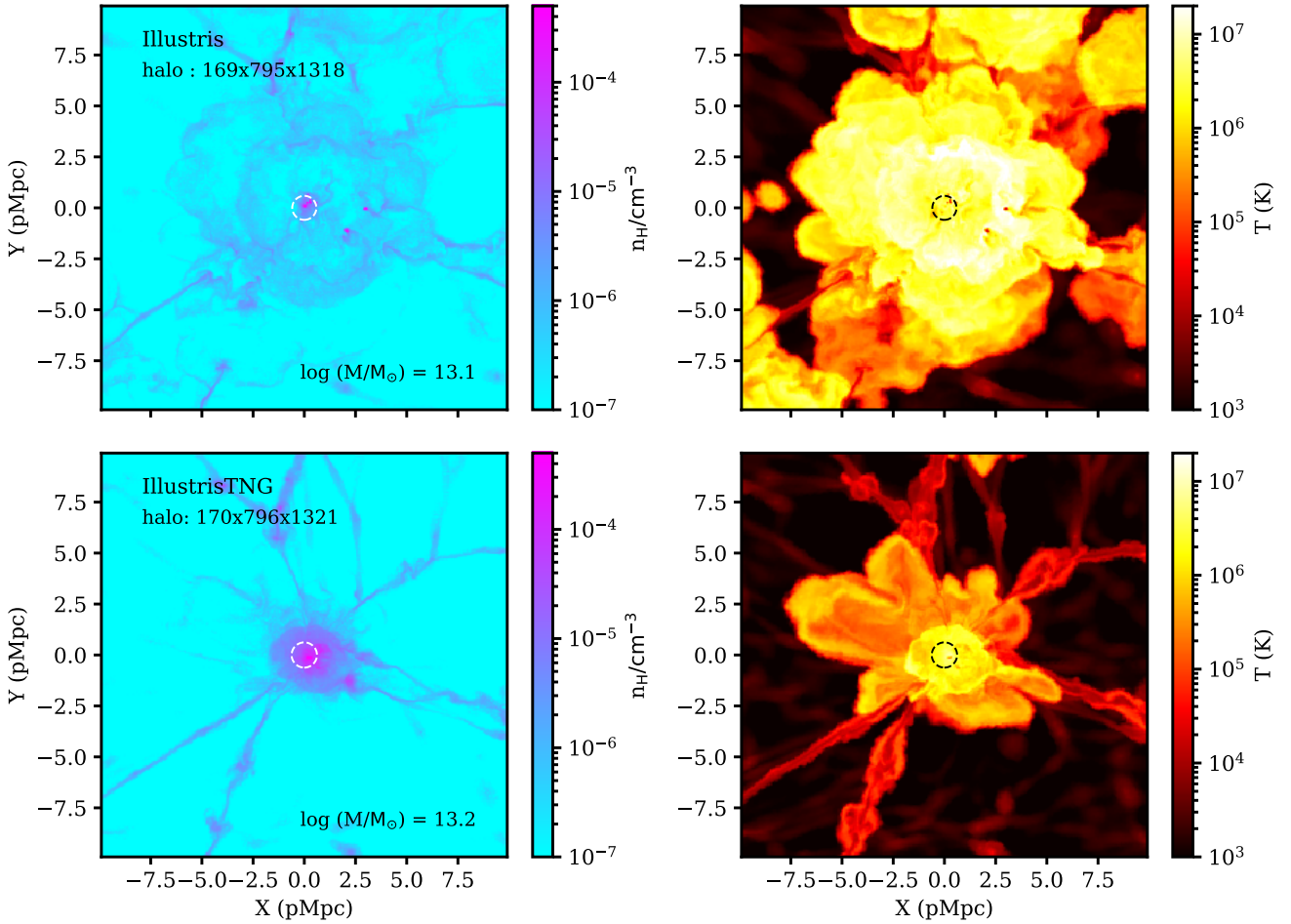


Figure 1. The figure shows the density (left) and temperature (right) of gas around the same halo at $z = 0.1$ in Illustris (top) and IllustrisTNG (bottom) simulation. Each panel represents a 2D slice of the simulation (with single cell width i.e. ~ 60 ckpc) centered at the position of the halo. The explosive radio-mode AGN feedback in the Illustris is responsible for displacing the hot gas to a large volume as compared to IllustrisTNG. Dashed circles at the center show the Virial sizes of halos. Both halos are identified by matching the coordinates of their location (as noted on the left-hand panels) from halo catalogs. Halo masses are noted in the legends.

to construct mock HST COS spectra, the automated Voigt profile fitting procedure, and the UV background calibration for both simulations.

3.1 Halo mass selection for LRG hosts

In this study, our primary objective is to assess how AGN feedback influences the gas surrounding halos within the Illustris and IllustrisTNG simulations. Given that AGN feedback is expected to suppress star formation in massive galaxies, particularly LRGs, we focus on massive halos capable of hosting LRGs. Observational evidence supports the idea that LRGs tend to reside in massive halos, as indicated by their clustering properties and abundance. To select suitable halos of LRGs from the simulations, we employ a simple model based on a step-function halo-occupation distribution. In this model, we assume that simulated halos above a specified mass threshold M_{\min} , are hosts to LRGs. We determine M_{\min} such that halos with $M > M_{\min}$ in our $z = 0.1$ Illustris and IllustrisTNG simulation boxes match with the measured

projected 2-point correlation function (2PCF) of LRGs at median redshift $z \sim 0.1$ obtained by Guo et al. (2015).

Because it is not straightforward to estimate the projected 2PCF in simulations, we relate the redshift-space projected 2PCF, $w_p(r_p)$, to the real-space correlation function $\xi(r_p)$ by following Zehavi et al. (2011),

$$w_p(r_p) = 2 \int_{r_p}^{\infty} r dr \xi(r) (r^2 - r_p^2)^{1/2}.$$

Then, for a power law $\xi(r_p) = (r/r_0)^{-\gamma}$ one obtains

$$w_p(r_p) = r_p \left(\frac{r_p}{r_0}\right)^{-\gamma} \Gamma(1/2) \Gamma\left(\frac{\gamma-1}{2}\right) / \Gamma(\gamma/2).$$

Using these relations we fit the $w_p(r_p)$ of Guo et al. (2015) for galaxies with magnitudes in SDSS r band $M_r < -21$. Our simple chi-by-eye fit gives us parameters $r_0 = 6.3$ and $\gamma = 1.9$. These values are also consistent with the fit obtained by Zehavi et al. (2011, $r_0 = 6.46$ and $\gamma = 1.9$ when using only diagonal elements for fit) for the galaxies with same M_r conditions.

We proceed by selecting halos with a mass $M > M_{\text{th}}$ from both simulations as given in their respective catalogs.

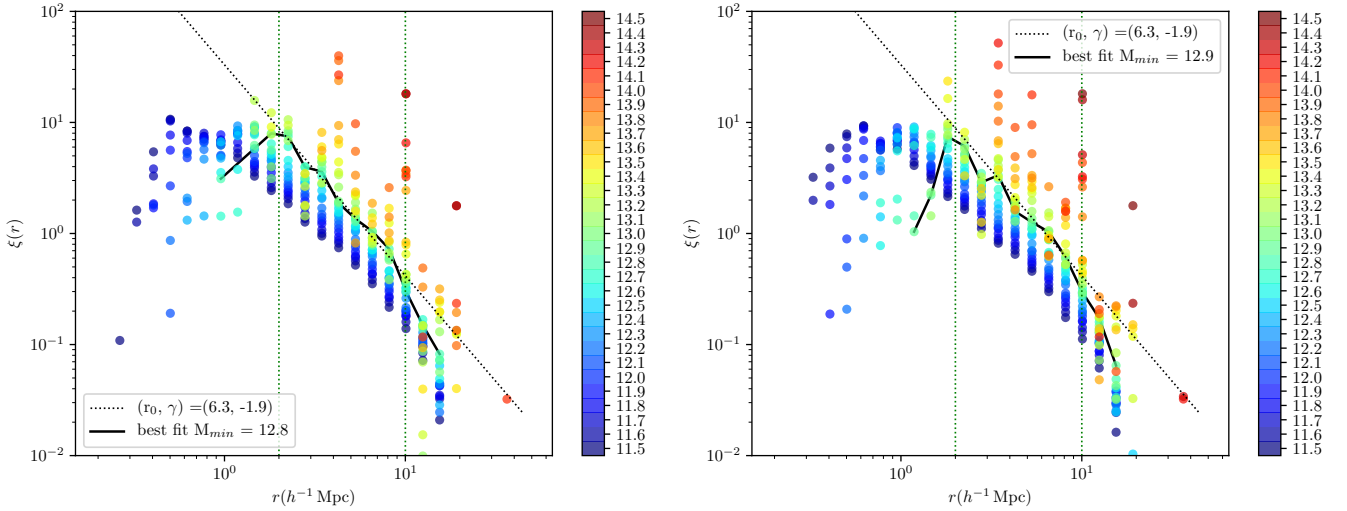


Figure 2. The projected 2-point correlation function $\xi(r)$ for Illustris (left-hand panel) and IllustrisTNG halos (right-hand panel) with mass ($M > M_{\min}$), as indicated by color-bars. The parametric fit form Guo et al. (2015) measurements (dotted line with slope) match with the best fit (solid lines) $M_{\min} = 10^{12.8} M_{\odot}$ for Illustris and $M_{\min} = 10^{12.9} M_{\odot}$ for IllustrisTNG. Vertical green dotted lines show the range of r used for obtaining the best fit M_{\min} values.

Subsequently, we compute the real-space correlation function, $\xi(r)$, for these halos using equispaced logarithmic bins over the range $0.01 < r (h^{-1} \text{ Mpc}) < 40$. The resulting correlations are shown in Fig. 2, where the color bar represents $\xi(r)$ values corresponding to different M_{th} . We compare this $\xi(r)$ with our power-law fit to the ξr from Guo et al. (2015) projected 2PCF measurements (dotted line in Fig. 2) and estimate the $M_{\min} = M_{\text{th}}$ for which the chi-square value is minimum. For minimizing chi-square we use bins of $0.01 < r (h^{-1} \text{ Mpc}) < 40$. This analysis yields values of $M_{\min} = 10^{12.8} M_{\odot}$ for Illustris and $M_{\min} = 10^{12.9} M_{\odot}$ for IllustrisTNG. These M_{\min} values align closely with the $M_{\min} = 10^{12.78 \pm 0.11} M_{\odot}$ value derived by Guo et al. (2015) for $M_r < -21$, employing more sophisticated halo occupation distribution modeling (refer to their table 2). These M_{\min} values yield a total of 296 halos in Illustris (for $M > 10^{12.8} M_{\odot}$) and 305 halos in IllustrisTNG (for $M > 10^{12.9} M_{\odot}$) at $z = 0.1$.

3.2 Generating Synthetic Ly α Forest around the halos and in the IGM

For generating synthetic Ly α forest, we need the temperature, density, and velocity of cells along the sightlines and the H I photoionization rate (Γ_{HI}) from the UV background to determine the neutral fraction of hydrogen. We generate two types of sightlines: one set passes in proximity to our chosen halos that host LRGs, known as halo sightlines, while the other set probes the IGM and is referred to as IGM sightlines. The IGM sightlines are just sightlines generated at random being agnostic to positions of halos.

For the IGM sightlines, we adopt the procedure outlined in Paper I. We draw 10^5 sightlines from one side of the simulation box to the other, parallel to an arbitrarily chosen z -axis. The starting points of these sightlines are chosen randomly on the $x-y$ plane.

To create halo sightlines, we generate sightlines around

halos hosting LRGs, aligned parallel to a chosen z -axis, at various impact parameters (r_{\perp}), representing the perpendicular distance from the halo center to the sightline. We establish 30 bins for impact parameters ranging from 0 to 90 pMpc, each with differing bin sizes. These bin sizes are designed to approximate equal logarithmic intervals in impact parameter space. When generating these sightlines, we ensure that the maximum number of sightlines within an impact parameter bin around all LRG halos totals 10^5 . To achieve this, we calculate the number of sightlines to be drawn around each halo in each impact parameter bin, which is given by $10^5/N_h$, where N_h represents the total number of halos in each simulation box with masses greater than M_{\min} . Subsequently, for each impact parameter bin surrounding each halo, we randomly generate $10^5/N_h$ sightlines that traverse the available cells within the $x-y$ plane. However, for the impact parameter bins closest to the halos, this value of $10^5/N_h$ is smaller than the number of available cells in the $x-y$ plane. Only in such cases, we generate sightlines that pass through all available cells within the annular ring defined by the edges of the respective impact parameter bins. For instance, in smaller impact parameter bins at $r_{\perp} < 0.5$ cMpc with a width of approximately 100 ckpc, the number of sightlines is less than 10^5 , and thus these sightlines are correlated. After creating the sightlines, we use periodic boundary conditions to center them at the real-space coordinate positions of the halos.

Along these halo and IGM sightlines, we store the values of temperatures T , overdensity Δ and the velocity component parallel to line-of-sight (v_z). In addition to these quantities, we also need neutral hydrogen fractions to generate the synthetic Ly α forest spectra. For that, we solve for a neutral fraction in ionization equilibrium including both collisional ionization and photoionization. At every cell along a line-of-sight, we use T , Δ , and Γ_{HI} to calculate the neutral fractions. We assume a constant value of Γ_{HI} for the whole simulation box. Specific values of Γ_{HI} used in Illustris and IllustrisTNG

are discussed in Section 3.3. For ionization equilibrium calculation we need an estimate of the electron density which can have a contribution of up to $\sim 16\%$ more from the ionization of helium gas. Following Paper I, we assume helium is predominantly in He III state and calculate the electron density. This approximation of complete ionization of helium is justified given that we are working at $z = 0.1$ which is almost 10 billion years after the epoch of helium reionization at $z \sim 3$ (Shull et al. 2010; Worseck et al. 2011; Khaira 2017). This assumption further helps in removing two free parameters, He I and He II photoionization rates, from ionization equilibrium calculation. Our calculations for ionization equilibrium incorporate revised cross-sections and recombination rates from Lukić et al. (2015). Additionally, we adopt the self-shielding approach outlined in Rahmati et al. (2013) for dense cells.

After determining the neutral fraction of hydrogen along a sightline, following procedure in Paper I (see also Hu et al. 2022, 2023) we use the values of T and v_z at each cell and calculate the Ly α optical depth τ at each cell by adding all the real space contributions to the redshift-based Ly α optical depth using complete Voigt profile (with approximation provided in Tepper-García 2006) arising from real-space cells. The continuum normalized flux is then just $F = e^{-\tau}$ along each sightline. We call these sightlines perfect Ly α forest sightlines. Pixel separation and hence the resolution of these sightlines is 4.12 km s^{-1} arising because we grid each simulation box into 1820^3 cells. This resolution of perfect sightlines is ~ 4 times finer than the resolution of HST-COS data ($\sim 15 - 20 \text{ km s}^{-1}$).

3.3 Forward models to determine photoionization rates

In Paper I, we emphasized the significance of adjusting Γ_{HI} in simulations to facilitate comparisons with low- z IGM observations (refer to section 4 of Paper I). This adjustment becomes especially crucial when comparing two simulations that exhibit distinct fractions of diffuse, low-temperature ($T < 10^5 \text{ K}$) gas responsible for observed Ly α absorption. As outlined in Paper I, Illustris contains 23.2% of baryonic mass in this diffuse Ly α phase, whereas IllustrisTNG has 38.5%. Therefore, we applied the same methodology detailed in Paper I to determine Γ_{HI} for both Illustris and IllustrisTNG. A concise summary of this procedure is provided below.

We created forward models with IGM sightlines drawn from simulations following the noise properties and convolution of lifetime position-dependent HST-COS LSF for Danforth et al. (2016) dataset in redshift bin $0.06 < z < 0.16$. This redshift bin contains 32 quasar spectra with $S/N > 10$ per pixel (of size 6 km s^{-1}) and the median of Ly α forest region covered in the redshift bin falls at $z = 0.1$. While creating forward models we stitched our IGM sightlines to cover the Ly α redshift path of each observed quasar spectra. We generate these forward models for different values of Γ_{HI} . We conducted Voigt profile fitting to all the Ly α lines falling in this redshift bin in the data as well as a set of forward models with our automatic python wrapper (developed in Hiss et al. 2018) that runs VPfit v10.2 (Carswell & Webb 2014)⁴. Using the results of fitting we calculate the Ly α line

number density dN/dz , i.e. the number of Ly α lines within a column density range per unit redshift for both simulations and the data. To be consistent with the results of Paper I, we choose the column density range for dN/dz to be $12 < \log N_{\text{HI}}(\text{cm}^{-2}) < 14.5$. In this specific column density range, we obtained $dN/dz = 205$ for the Danforth et al. (2016) dataset within the redshift bin $0.06 < z < 0.16$. We determine the best fit Γ_{HI} for both simulations that matched well with the dN/dz of the data. We found $\Gamma_{\text{HI}} = 3.1 \times 10^{-12} \text{ s}^{-1}$ for Illustris and $7.73 \times 10^{-12} \text{ s}^{-1}$ for IllustrisTNG, as found in (refer to Section 4 of) Paper I. For the subsequent analysis presented in this paper, we use these values of Γ_{HI} for both IGM and halo sightlines, unless otherwise specified.

3.4 Forward models for halo and IGM sightlines motivated by archival data

Motivated by large differences in the temperature and density of gas around halos in the Illustris and IllustrisTNG simulation, we wish to investigate if Ly α forest around those halos shows significant differences so that we can use it to constrain feedback models. Moreover, in order to study the feasibility of using Ly α forest around halos to constrain the feedback, we want to find out the properties of the data that is already available in the archive so that we can approximate our forward models accordingly. Therefore, we mined the HST spectroscopic legacy archive (HSLA; Peebles et al. 2017) and searched for background quasar spectra which have Ly α forest with $S/N > 5$ per resolution element of COS (with FWHM of $\sim 18 \text{ km s}^{-1}$). Then we used the SDSS DR12 LRG catalog (Tojeiro et al. 2012) to cross-match these quasar sightlines with LRGs. We identified 3193 quasar-LRG pairs where each background quasar probes the Ly α forest at the redshift of one or more foreground LRGs at impact parameters in the range $0.1 \text{ pMpc} < r_{\perp} < 10 \text{ pMpc}$. This means we select LRGs with redshift $z_{\text{LRG}} < z_q$, where z_q is the redshift of the background quasar. Our selected 3193 LRGs are being probed by 94 HSLA quasar spectra observed by FUV gratings of HST COS. The mean S/N per resolution element of the COS in the Ly α forest across the entire dataset is 12.8 which corresponds to S/N of 7.4 per pixel of size $\Delta v = 6 \text{ km s}^{-1}$ as used in Danforth et al. (2016) binned data. The redshift distribution of these foreground 3193 galaxies and their impact parameter from the 94 background quasar sightline probing Ly α forest is plotted in Fig. 3. The redshift distribution of galaxies peaks at $z \sim 0.1$ and therefore aligns well with our simulation box redshift. Our choice of impact parameter range up to 10 pMpc is motivated by the significant differences seen in the temperature and density profile of massive halos up to 10-20 pMpc as shown in Fig. 1.

Our selected quasar-LRG sample includes data from past HST COS programs that specifically targeted quasars near LRGs (Chen et al. 2018, 2019; Zahedy et al. 2019; Berg et al. 2019). However, it is worth noting that these prior studies primarily focused on regions within $r_{\perp} \lesssim R_{\text{vir}} \simeq 0.5 \text{ pMpc}$, concentrating on the CGM and metal lines. In contrast, our investigation extends to much larger impact parameters, reaching up to 10 pMpc.

Given these properties of quasar-LRG pairs from archival data, we adopt a simple approach of modeling Ly α forest in the halo and IGM sightlines with $S/N = 7$ per pixel (of $\Delta v = 6 \text{ km s}^{-1}$). Furthermore, for simplicity, we assume all

⁴ see <http://www.ast.cam.ac.uk/rfc/vpfit.html>

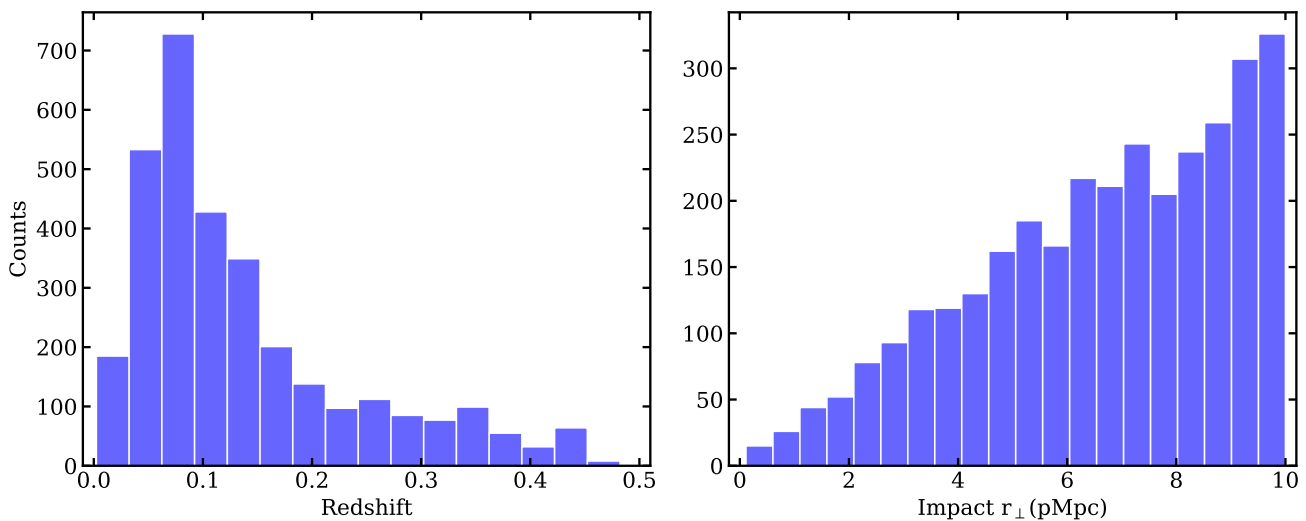


Figure 3. Redshift (left) and impact parameter (r_{\perp} , right) distribution of the 3193 foreground SDSS LRGs as probed by 94 background quasar spectra from the HSLA. These sightlines are selected to have spectra with $S/N > 5$ per COS resolution element in the Ly α forest region (with sample mean of $S/N = 12.8$ per COS resolution element).

3193 LRGs are at a single redshift $z = 0.1$ which is also the median of the redshift distribution (see left-hand panel of Fig. 3), so that we can just analyze a single snapshot of both simulations used here at $z = 0.1$. For the generation of these forward models, we first convolve our perfect sightlines with HST-COS G130M grating LSF that covers Ly α forest at $z = 0.1$ and then rebin the spectrum to match the pixel separation given in Danforth et al. (2016) paper (i.e with a pixel velocity scale of 6 km s^{-1}) and then add Gaussian random noise at each pixel to get the S/N of 7 per pixel.

After creating forward-modelled halo sightlines, we fit them with our automated VPfit code to obtain b and N_{HI} for all the Ly α absorption lines falling within $\pm 500 \text{ km s}^{-1}$ centered at the position of halos. Our choice of this velocity width, $\pm 500 \text{ km s}^{-1}$ along the sight-line, is an arbitrary choice only motivated to keep a large enough spectral chunk to probe Ly α forest lines far away from halos. Additionally, this choice allows us to account for lines that may be offset from the center of the halos due to the high-velocity gradients near these structures. In order to choose $\pm 500 \text{ km s}^{-1}$ velocity windows, the center of the sightline is determined by the real space position of the halo on z -axis, subtracted by the z -component of the peculiar velocity of halo. This centering method resembles the procedure followed in the observations of background quasar absorption lines probing the halo of a foreground galaxy.

In Fig. 4, we show a portion of two such examples sightlines passing through the same locations around the same halos in Illustris (left-hand panel) and IllustrisTNG (right-hand panel) at an impact parameter $r_{\perp} = 1.3 \text{ pMpc}$. The top panel shows our forward model as well as perfect Ly α absorption spectra. Blue ticks show the Ly α absorption lines identified by our automated VPfit, while the two numbers in bracket indicate b in km s^{-1} and $\log(N_{\text{HI}}/\text{cm}^{-2})$. Within a velocity window $\pm 500 \text{ km s}^{-1}$ centered on the position of halos (cyan shaded region), VPfit identifies one Ly α absorption lines for the sightline passing through the halo of Illustris and two Ly α absorption lines for sightline passing through

the halo of IllustrisTNG. Fig. 4 also shows the temperature and density, and corresponding optical depth weighted quantities (refer to equation 1 of Paper I), along the sightlines. It shows that the gas is much hotter ($10^6 - 10^7 \text{ K}$) around the Illustris halos and extends up to a large distance because of the aggressive bubble-radio mode feedback as compared to the IllustrisTNG. This is responsible for the difference in the number of lines identified by VPfit. The velocity v_z parallel to z -axis, as shown in the fourth panel (from the top) of the figure, illustrates the regions that are affected by the feedback. Large velocity gradients in Illustris as compared to IllustrisTNG show that the strong feedback in the former is displacing gas violently around the halo. Whereas far away from the halo, at large v_z , velocity profiles of both simulations are similar. The last panel in the figure indicates the ionization fraction of neutral hydrogen X_{HI} for each cell. The X_{HI} illustrates the fact that in the region around halos, it is the combination of high over-densities and low temperature that give rise to higher X_{HI} values, of the order of 10^{-5} , responsible for imprinting the Ly α absorption lines on the sightlines. Given that the temperatures are lower around IllustrisTNG halos, more Ly α absorption lines are imprinted on sightlines. There are also some very broad but weak lines appearing on the perfect sightline because of very high-density high-temperature gas near the halo, however, they are not identified by VPfit in forward-modeled spectra because of the finite S/N .

As shown in the example (Fig. 4), we Voigt profile fit all the halo sightlines as well as IGM sightlines and obtain the b and N_{HI} for each Ly α line detected by our automated routine. Using these we study different statistics of gas around halos as a function of r_{\perp} . These are discussed in the following section.

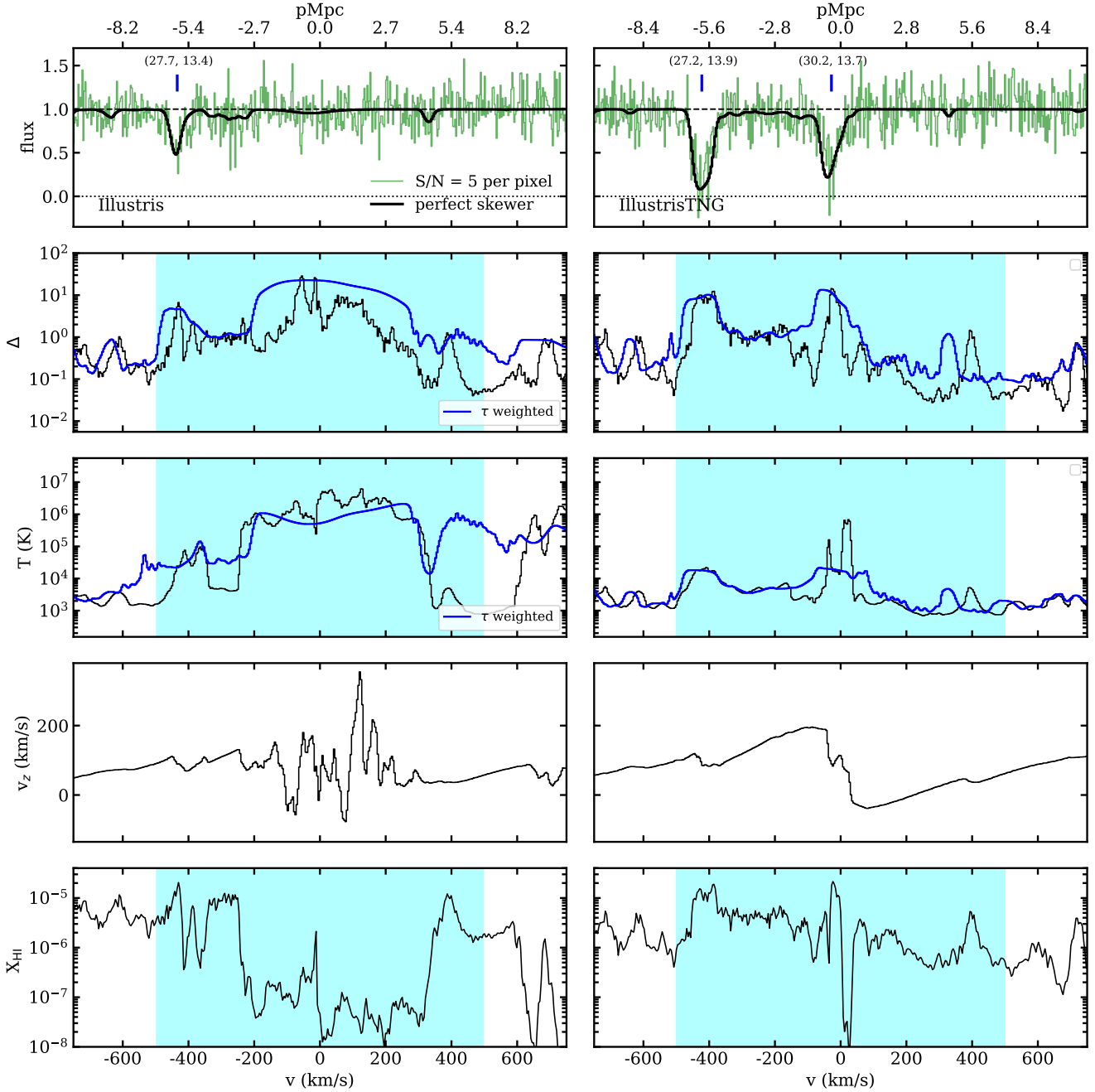


Figure 4. A representative example of Ly α forest sightlines at $r_{\perp} \sim 1.3$ pMpc around the same halo in Illustris (left-hand panels) and IllustrisTNG (right-hand panels). From the top, black lines show the normalized flux (perfect spectra), overdensity (Δ), temperature, line of sight velocity (v_z) and HI fraction along the sightline. Green histograms on top panels show the HST-COS forward modeled sightlines with S/N = 7 per pixel (of size $\Delta v = 6$ km s $^{-1}$). The blue ticks indicate VPfit identified Ly α -absorption lines and legends in the bracket show the values of fitted b (km s $^{-1}$) and $\log(N_{\text{HI}}/\text{cm}^{-2})$, respectively. Blue curves in the second and third panels from the top show optical depth weighted overdensities and temperature respectively. Because the gas is much hotter for Illustris just one Ly α absorption line has been identified in the forward-modeled spectra as compared to two lines for IllustrisTNG within ± 500 km s $^{-1}$ window highlighted by shaded cyan color. Different sizes of the sightlines on the left and right panel (as noted on top x-axis) is a consequence of the different values of Hubble constants used in the simulations (see Table 1).

4 IMPACT OF AGN FEEDBACK ON THE GAS AROUND LRGS

In this section, we describe the results of our Voigt profile fitting of the Ly α lines near halos at different impact parameters and study the feasibility of using those as a diagnostic

tool to probe the impact of AGN feedback. For this, we use the joint and marginalized distribution of b and N_{HI} and dN/dz with impact parameter r_{\perp} as summary statistics. The results of those are described in the following subsections.

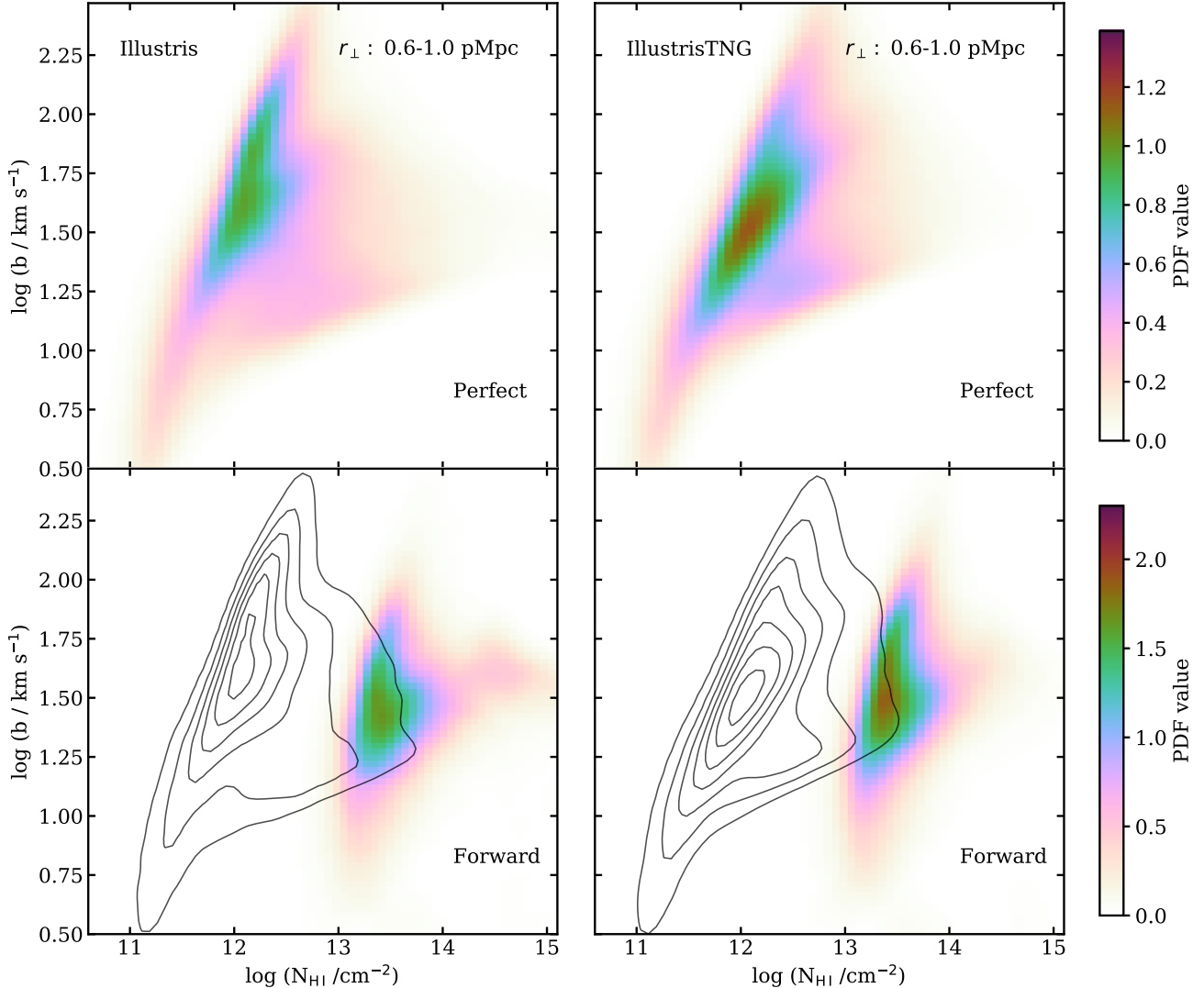


Figure 5. The KDE estimated 2D b – N_{HI} distribution for the halo sightlines (within $\pm 500 \text{ km s}^{-1}$) drawn from the impact parameter bin $0.6 < r_{\perp} < 1 \text{ pMpc}$ of Illustris (left-hand panel) and the IllustrisTNG (right-hand panel) halos for perfect (top) and forward (bottom) models. The distributions from perfect and forward models look similar except the normalization shown with colors. In the bottom panel, we show b – N_{HI} distribution from perfect models with contours. The forward models shift b – N_{HI} distribution towards higher N_{HI} and lower b values in both simulations.

4.1 The b – N_{HI} distribution around halos

We select a central velocity window of $\Delta v_z = \pm 500 \text{ km s}^{-1}$ of halo sightlines and store the b and N_{HI} values of the Ly α absorption lines identified and fitted by VPfit for forward modeled as well as perfect Ly α forest spectra. As in the Paper I, for perfect spectra, we add a small Gaussian random noise (which gives $S/N = 100$ per pixel of size 4.2 km s^{-1}) so that VPfit can robustly identify lines. Without such a noise, VPfit fails to identify many Ly α lines. This is because VPfit identifies lines bound by flux equal to unity and for most of the regions in the perfect sightlines the flux is smaller than unity by a tiny amount of 10^{-3} to 10^{-5} . We mitigate this issue by adding a very small noise so that the flux becomes unity and VPfit can identify lines. Once we fit those lines, we use the b and N_{HI} values to calculate 2D b – N_{HI} distribution with Gaussian KDE at different impact parameters around massive halos of Illustris and IllustrisTNG.

In Fig. 5 we show the normalized 2D KDE b – N_{HI} distributions for Illustris (left-hand panels) and IllustrisTNG (right-hand panels) at an impact parameter bin of $0.6 < r_{\perp} < 1 \text{ pMpc}$ from selected halos. This impact bin is 1 to 2 Virial radii from the halos of the given M_{min} mass. The top panels show the b – N_{HI} distributions obtained with perfect sightlines ($S/N = 100$ and $\Delta v = 4.2 \text{ km s}^{-1}$). The shape of the distribution is qualitatively similar for both simulations showing a higher density of lines with $\log(b/\text{km s}^{-1}) > 1.25$ and $\log(N_{\text{HI}}/\text{cm}^{-2}) > 11.5$. The similar shapes of the distribution suggest that at very close to the halos, the temperature and density of gas in both simulations are similar (see for e.g Fig. 1). However, the normalization of the distribution which is indicated by the color bar in Fig. 7 shows that there are more lines in IllustrisTNG than in Illustris. Note that in these perfect spectra VPfit could identify large $\log(b/\text{km s}^{-1})$ upto ~ 2.5 (i.e $\sim 300 \text{ km s}^{-1}$). In the bottom panel of Fig. 5

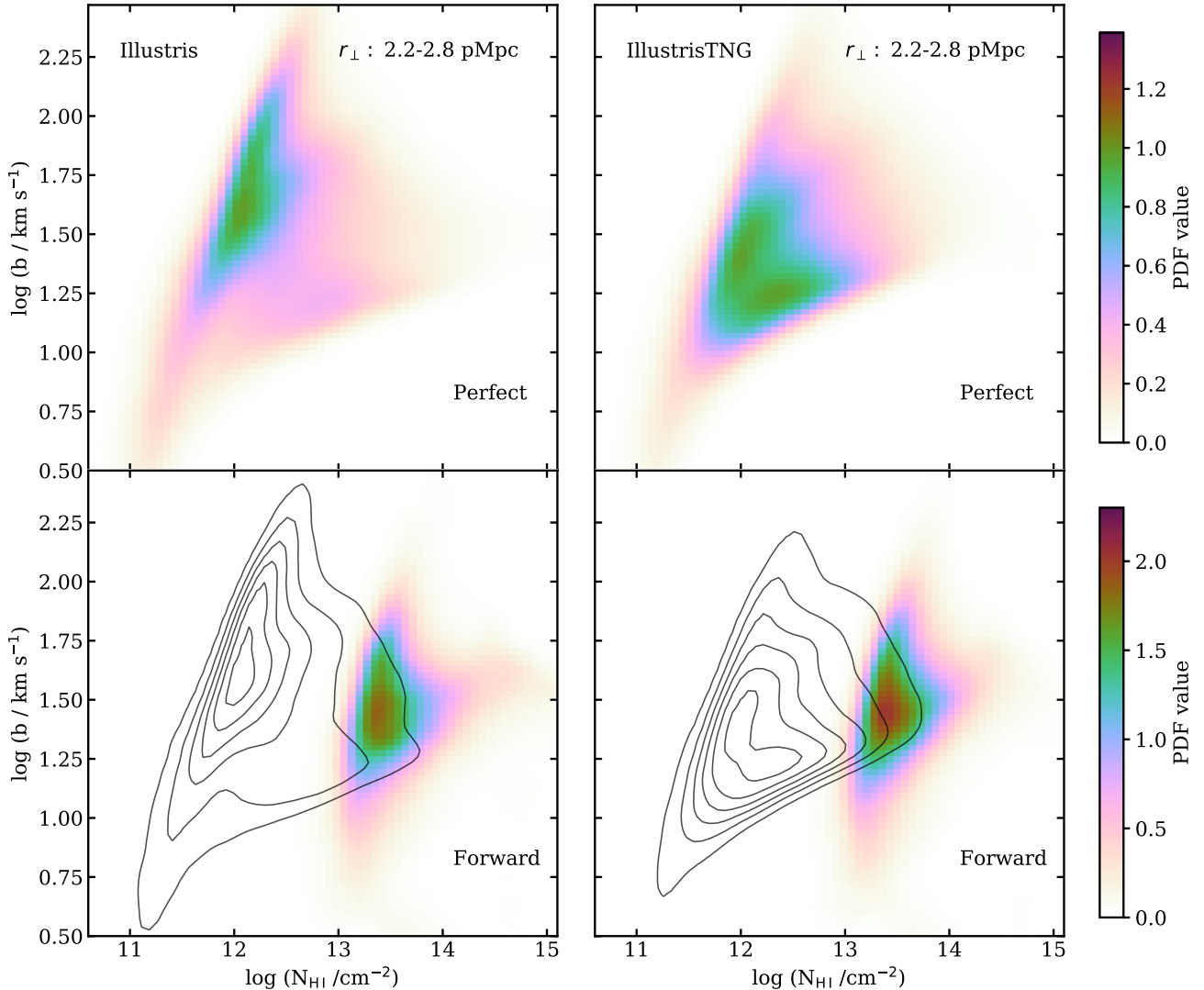


Figure 6. The KDE estimated 2D b - N_{HI} distribution for the halo sightlines (within $\pm 500 \text{ km s}^{-1}$) drawn from the impact parameter bin $2.2 < r_{\perp} < 2.8 \text{ pMpc}$ of Illustris (left-hand panel) and the IllustrisTNG (right-hand panel) halos for perfect (top) and forward (bottom) models. The effect of feedback can be seen in the difference in the distributions (in top panels) for perfect sightlines. The hot gas in the Illustris results in many absorption lines with low N_{HI} high and b values whereas the IllustrisTNG shows both the low N_{HI} -high b and high N_{HI} -low b absorption lines. These differences in the shape of b - N_{HI} get washed out in forward-modelled sightlines as shown in the bottom panel where the black contours indicate distribution from the perfect model shown on the top panel. However, the normalization of distribution showing different numbers of lines, indicated by the color bars is still significantly different even in the distribution from forward-modelled sightlines.

we plot b - N_{HI} distributions obtained with forward modelled Ly α forest spectra. Here also, the shapes of distributions from both simulations seem to agree qualitatively. For comparison with results from perfect sightlines, the bottom panels also show the b - N_{HI} distributions from the perfect model (as plotted in the top panels) with contours. As compared to those contours, the b - N_{HI} distributions from forward models shift towards higher values in $\log(N_{\text{HI}}/\text{cm}^{-2}) > 13$. Even here with noisy forward models, the normalization is different between the two simulations showing that there are more Ly α lines in IllustrisTNG than in Illustris. However, in these noisy spectra VPfit could identify $\log b$ values up to ~ 2 (i.e. $\sim 100 \text{ km s}^{-1}$), significantly smaller than in the case of perfect sightlines. This suggests that there are many broad lines

that are too shallow to get detected by VPfit in forward-modelled spectra. Another interesting weak trend seen in these plots is there are more lines at higher $\log(b/\text{km s}^{-1}) > 2$ values in IllustrisTNG than in Illustris. It is mainly because the gas temperatures in IllustrisTNG especially for hot gas ($T > 10^{5.5} \text{ K}$) are lower than Illustris (as can be seen in Fig. 1 and temperature density phase diagram shown in Paper I) which can imprint deeper broad lines that are easily detected by VPfit.

Similar to Fig. 5, in Fig. 6 we plot normalized 2D KDE b - N_{HI} distributions at an intermediate impact parameter $2.2 < r_{\perp} < 2.8 \text{ pMpc}$ from massive halos in both simulations. Unlike the case with a small impact parameter (shown in Fig. 5) the b - N_{HI} distributions for perfect Ly α forest spectra show

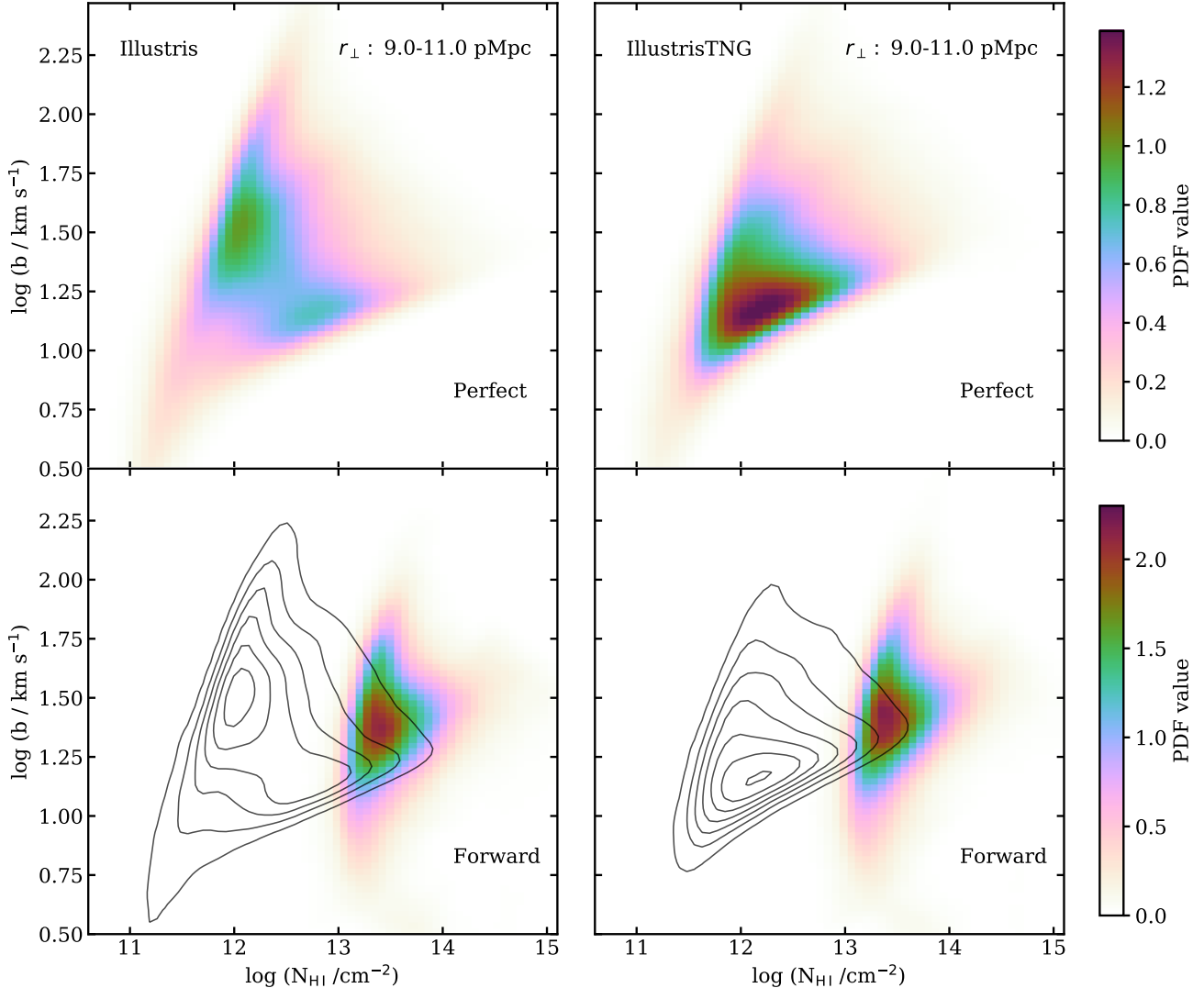


Figure 7. The KDE estimated 2D b - N_{HI} distribution for the halo sightlines (within $\pm 500 \text{ km s}^{-1}$) drawn from the impact parameter bin $9 < r_{\perp} < 11 \text{ pMpc}$ of Illustris (left-hand panel) and the IllustrisTNG (right-hand panel) halos for perfect (top) and forward (bottom) models. The effect of feedback can be seen in the difference in the distributions (in top panels) for perfect sightlines. As compared to the b - N_{HI} distribution obtained for low (Fig. 5) and intermediate (Fig. 6) r_{\perp} bins there are more lines at high- N_{HI} low lower- b values in Illustris whereas most of the lines in IllustrisTNG are at high- N_{HI} low lower- b values. For forward-modelled sightlines, the b - N_{HI} distributions are indistinguishable and close to the distribution observed for the IGM (see Paper I). See Fig. A1 and A2 for b - N_{HI} at other r_{\perp} bins.

clear differences. IllustrisTNG b - N_{HI} distribution is bimodal and it clearly shows two lobes one at $\log(b/\text{km s}^{-1}) > 1.25$ and another at $\log(b/\text{km s}^{-1}) < 1.25$, where former is mainly at lower column densities ($\log(N_{\text{HI}}/\text{cm}^{-2}) < 12.3$) and latter is at high column densities ($\log(N_{\text{HI}}/\text{cm}^{-2}) > 12$). Whereas Illustris just has one prominent region at $\log(b/\text{km s}^{-1}) > 1.25$ and it is remarkably similar to the one at lower impact parameter (see Fig. 5). This is mainly because there is no significant difference in the temperature and density profile in Illustris halos till such a large (up to $\sim 3 \text{ pMpc}$) impact parameters as illustrated in one example of temperature and density profile around halos in Fig. 1. Note the highest b values probed by IllustrisTNG is now lower than Illustris suggesting that the temperatures are significantly lower around these impact parameters in IllustrisTNG. Bottom panels of Fig. 6 compare b - N_{HI} distributions from forward modeled Ly α forest spec-

tra. The trends are similar to what is seen in the case of lower impact parameters (see, bottom panel of Fig. 5) but there is a less prominent difference in the normalization. It shows there is still a difference in the number of Ly α absorption lines but not as high as seen in the case of a lower-impact parameter.

Similar to Fig. 5 and Fig. 6, in Fig. 7 in we plot normalized 2D KDE b - N_{HI} distributions at a large impact parameter $9 < r_{\perp} < 11 \text{ pMpc}$ from massive halos in both simulations. The b - N_{HI} distributions for perfect Ly α forest spectra show clear differences between both simulations and they are in very good agreement with the ones obtained for IGM (as shown in Fig. 4 of Paper I). As compared to lower and intermediate impact parameters (Fig. 5 and Fig. 6) Illustris shows many lines with lower b values ($\log(b/\text{km s}^{-1}) < 1.75$) and there are many more lines with

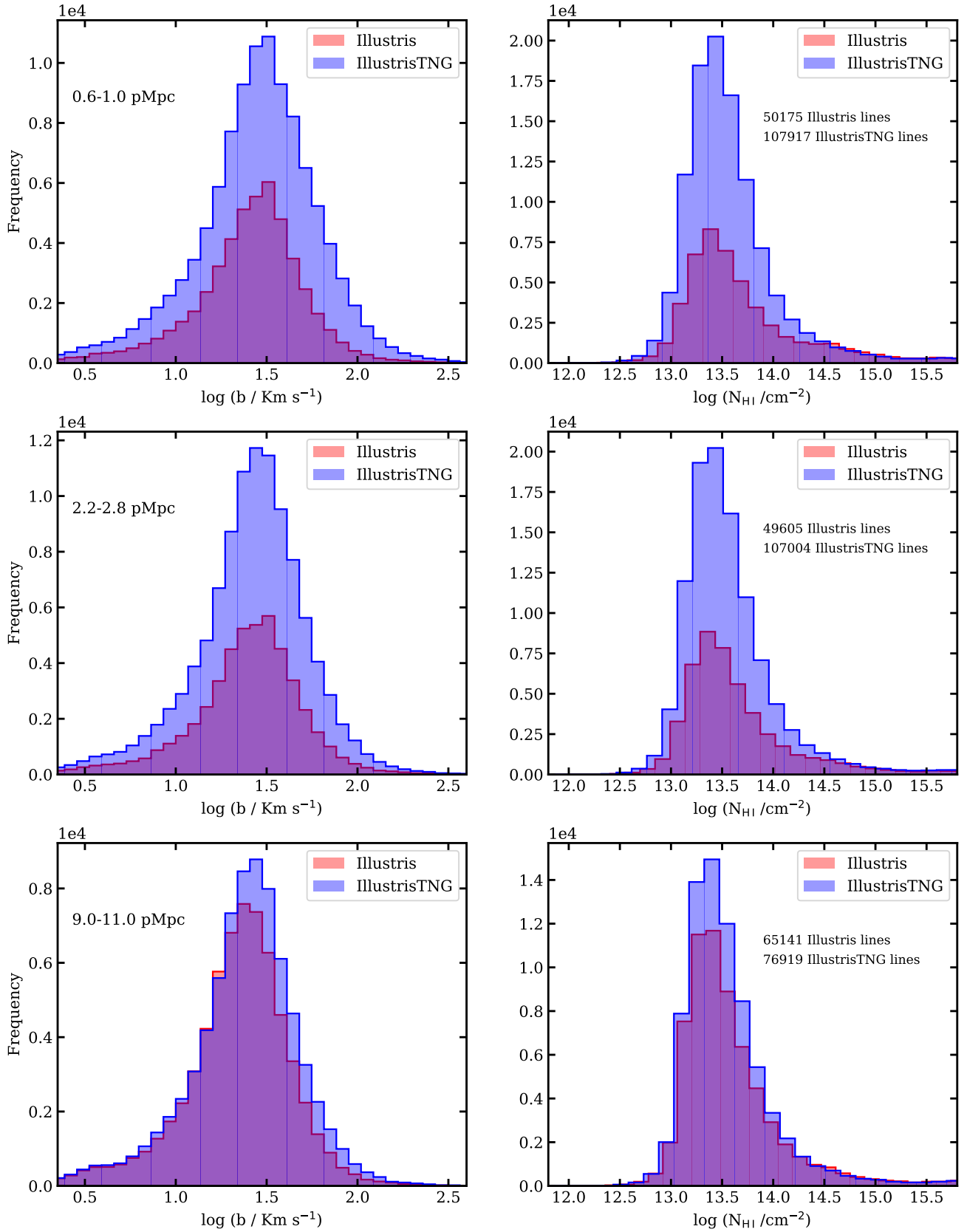


Figure 8. The $\log b$ (left) and $\log N_{\text{HI}}$ (right) distribution from the forward modeled sightlines generated at a low impact parameter bin $0.6 < r_{\perp} < 1.0$ pMpc (top panel), at an intermediate impact parameter bin $2.2 < r_{\perp} < 2.8$ pMpc (middle panel) and at high impact parameter bin $9 < r_{\perp} < 11$ pMpc (bottom panel). Distribution is not normalized and the number of total Ly α lines in each bin are indicated in left-hand panels. Both simulations use the same number of sightlines ($\sim 10^5$) in each r_{\perp} bin. See Fig. A3 and A4 for other r_{\perp} bins.

high column densities $\log(N_{\text{HI}}/\text{cm}^{-2}) > 12.5$ and small b values ($\log(b/\text{km s}^{-1}) < 1.25$). In the case of IllustrisTNG however, the b - N_{HI} distribution shows that most of the Ly α absorption lines are at small b values $\log(b/\text{km s}^{-1}) < 1.4$ and high column densities $\log(N_{\text{HI}}/\text{cm}^{-2}) > 12$. As expected from density and temperature profiles of typical halos, a comparison of b - N_{HI} distributions with impact parameters (Fig. 5, Fig. 6 and Fig. 7), shows that with increasing impact parameters the Ly α absorption lines become narrow (decrease in b values) and contain more neutral hydrogen gas (increase in N_{HI}). This trend is seen in both simulations but it is more prominent in the case of IllustrisTNG. To further illustrate such a trend we show b - N_{HI} distributions at different impact parameters in Appendix (Fig. A1 and A2). Very close to the halos at lower impact parameters, the shape of the b - N_{HI} distributions are similar in both simulations and they start differing as the impact parameters are increased. The b - N_{HI} distribution in both simulations nicely converges to the distributions in the IGM at large impact parameters ($r_{\perp} > 10$ pMpc). Bottom panels of Fig. 7 compare b - N_{HI} distributions from forward modelled Ly α forest spectra. Similar to lower and intermediate impact parameters (bottom panels of Fig. 5 and Fig. 6) the b - N_{HI} distributions show that most of the Ly α absorption lines are at higher column densities ($\log(N_{\text{HI}}/\text{cm}^{-2}) > 13$) spanning a limited range in b in both simulations. The distribution shapes and even the normalization indicated by the color bar look similar. This shows that the differences seen in the b - N_{HI} distributions obtained with both perfect and forward modeled Ly α spectra are washed out at these large impact parameters (~ 10 pMpc) from massive halos. Also the b - N_{HI} distribution is in very good agreement with the one seen in the case of IGM (see Paper I) suggesting that at high-impact parameters we are probing the gas residing mainly in the IGM (also see Fig. A1 and A2 in Appendix).

As shown in the Paper I, the shape of the b - N_{HI} distributions for IGM obtained from perfect Ly α forest spectra ($S/N = 100$ per pixel and $\Delta v = 4.2$ km s $^{-1}$) can distinguish the effect of feedback. The same is true for the shape of the b - N_{HI} distributions around massive halos for impact parameters of $\gtrsim 1.5$ pMpc. This signal in shape, however, gets washed out in forward-modeled Ly α spectra but the number of Ly α absorption lines show significant differences till impact parameters of ~ 10 pMpc in both perfect as well as forward modeled Ly α forest.

Given that the main difference in b - N_{HI} distributions between two simulations from forward modeled Ly α forest is in the number of Ly α absorption lines, in Fig. 8 we plot the individual histograms of b (left-hand panels) and N_{HI} (right-hand panels) at the same impact parameter bins for which the b - N_{HI} distributions are plotted in Fig. 5, 6 and 7. These histograms are plotted from $\sim 10^5$ forward modeled Ly α forest spectra around halos in each simulation. At all impact parameter bins, the shapes of both b and N_{HI} histograms are identical but there is a clear difference in the amplitude showing the difference in the number of Ly α absorption lines detected by VPfit. For reference, the number of Ly α lines plotted in the histogram is indicated on the right-hand panel of Fig. 8. At small and intermediate impact parameter bins (top and middle panel), the number of Ly α lines in IllustrisTNG is higher than Illustris by a factor of ~ 2 . Whereas at large impact parameters of 10 pMpc (bottom panel) Illus-

trisTNG shows only 18 percent more Ly α lines than Illustris. To further investigate the trend in the number of Ly α lines detected, we show individual histograms of b and N_{HI} distributions at different impact parameters in Fig A3 and A4 in the Appendix. These plots and the difference in the number of lines detected in each bin illustrate a trend where there are large differences in the detected Ly α lines at lower impact parameters and with increasing impact parameter this difference diminishes. This is expected since at high-impact parameters from halos we are probing the regions in the IGM and we expect the number of lines for the same redshift path length should be the same since we calibrated both simulations with Γ_{HI} values via matching the dN/dz .

Given the prominent difference in the number of Ly α lines detected as a function of impact parameter, we now focus on the simple statistics of line density profile around massive halos $dN/dz(r_{\perp})$, as discussed in the following subsection.

4.2 The line density profile around halos

The line density profile around halos, $dN/dz(r_{\perp})$, is the number of Ly α absorption lines within some N_{HI} range per unit redshift pathlength as a function of r_{\perp} . In our forward models, we are sensitive to the $N_{\text{HI}} \sim 10^{12.5}$ cm $^{-2}$, and the lines above $N_{\text{HI}} > 10^{14.5}$ cm $^{-2}$ are usually saturated. However, to be consistent with N_{HI} range that is used for the analysis in Paper I and for tuning the values of Γ_{HI} here (in section 3.3), we choose the range of $10^{12} < N_{\text{HI}} < 10^{14.5}$ cm $^{-2}$ for $dN/dz(r_{\perp})$ calculation. At each impact parameter bin centered at r_{\perp} we count all the Ly α lines ($N_{\text{Ly}\alpha}$) within the velocity range $\Delta v_z = \pm 500$ km s $^{-1}$ as identified by VPfit falling in our column density range. We calculate the total path length Δz covered by the sightlines in each impact parameter bin by multiplying the number of sightlines in the bin (N_{fit}) by the redshift path of a single sightline i.e. the redshift path Δz_{1000} for the central 1000 km s $^{-1}$ segment of the sightlines since we only count lines in the velocity range $\Delta v_z = \pm 500$ km s $^{-1}$. For this calculation, we use the same cosmological parameters with which the simulations are run and measure the line density at each impact parameter bin as $dN/dz = N_{\text{Ly}\alpha}/(N_{\text{fit}}\Delta z_{1000})$. In this way, we calculate dN/dz at different r_{\perp} bins from 0.1 to 90 pMpc 5 in Illustris and IllustrisTNG.

In order to compute the dN/dz from ambient IGM we generate forward-modeled IGM sightlines. We follow the same forward modeling procedure as in the case of halo sightlines as explained in Section 3.4. These are randomly drawn sightlines and we do not restrict to a velocity window, rather we use full sightlines. As expected we find dN/dz values for the IGM (with the same $10^{12} < N_{\text{HI}} < 10^{14.5}$ cm $^{-2}$ range) for both Illustris ($dN/dz = 71.5$) and IllustrisTNG ($dN/dz = 72.3$) to be essentially the same, i.e. the difference is within 1.1%. This is expected because we have calibrated Γ_{HI} by matching dN/dz of IGM (see Section 3.3). However, note that the dN/dz values quoted here (71.5 and 72.3) are different from the one we used ($dN/dz = 205$) from Paper I to calibrate the Γ_{HI} using Danforth et al. (2016) data (Section 3.3) because the

⁵ We chose 23 r_{\perp} bins of variable sizes to accommodate a sufficiently large number of sightlines (up to 10^5) to have precise dN/dz .

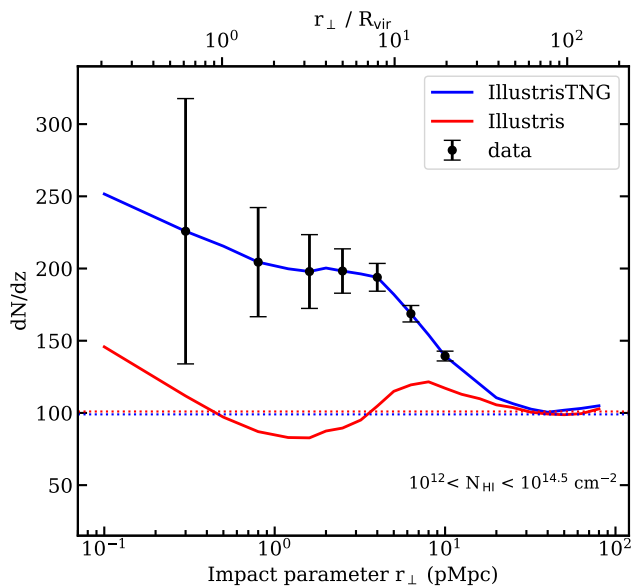


Figure 9. The line density profile $dN/dz(r_{\perp})$ for $10^{12} < N_{\text{HI}} < 10^{14.5} \text{ cm}^{-2}$ absorbers obtained from forward modeled mock spectra around LRG host halos within $\pm 500 \text{ km s}^{-1}$ along line-of-sights. IllustrisTNG (blue) gives a factor of $\sim 1.5 - 2$ higher dN/dz as compared to Illustris (red) out to $r_{\perp} \lesssim 5 \text{ pMpc}$ ($\sim 10R_{\text{vir}}$). By construction, both simulations converge to the expected IGM dN/dz (dotted lines) at large distances from halos. The black points with error bars show the expected precision using archival data assuming IllustrisTNG is the true model (see section 4.3 for more details). With this data, we can distinguish between Illustris and IllustrisTNG feedback models at 12σ statistical significance.

forward models are different in both cases. Here we use $S/N = 7$ per pixel (of 6 km s^{-1} ; 12.2 per resolution element) same for all sightlines but for Danforth et al. (2016) data we had different S/N in each quasar spectrum. For Danforth et al. (2016) data we used the condition $S/N > 17$ per resolution element (i.e. $S/N > 10$ per pixel of 6 km s^{-1}), same as done for $\text{Ly}\alpha$ forest power spectrum calculation in Khaira et al. (2019). It is reassuring that our calibrated Γ_{HI} results in same dN/dz for both simulation irrespective of the S/N of data used for calibration.

In Fig. 9 we plot the $dN/dz(r_{\perp})$ from the forward modelled $\text{Ly}\alpha$ forest in both simulations up to $r_{\perp} = 90 \text{ pMpc}$. The top axis shows r_{\perp}/R_{vir} where we use a representative value of $R_{\text{vir}} = 0.49 \text{ pMpc}$ obtained for the $z = 0.1$ halo with mass $10^{12.9} M_{\odot}$ which is the threshold M_{min} for IllustrisTNG LRG hosts. To understand the interesting trends seen in $dN/dz(r_{\perp})$, in Fig. 10 we plot the median values of the optical depth weighted temperature (T_{τ}) and over-densities (Δ_{τ}), and mean flux at different r_{\perp} calculated over the same $\pm 500 \text{ km s}^{-1}$ window. As expected, both simulations show that dN/dz (in Fig. 9) to be higher near halos and it decreases monotonically at larger r_{\perp} up to 1 pMpc (i.e. $\sim 2R_{\text{vir}}$). This has been ubiquitously seen in the CGM observations in various surveys (e.g. Werk et al. 2012; Chen et al. 2018). The decline in dN/dz seen here is mainly because of the decline in the gas density with r_{\perp} as shown in the middle panel of Fig. 10. Whereas, the temperatures are almost the same up until $\sim 2R_{\text{vir}}$ in both simulations (left panel of Fig. 10) because of the viral shocks near halos. This is more evident when we compare the

decline in median T_{τ} and Δ_{τ} in both simulations. For example, Fig. 10 shows that up to $r_{\perp} = 1 \text{ pMpc}$, the median Δ_{τ} drops by an order of magnitude in the case of IllustrisTNG whereas the drop in median T_{τ} is of the factor of only $\sim 3 - 4$. In the case of the Illustris simulation, median Δ_{τ} drops by a factor of ~ 3 (i.e. 0.5 dex) but the median T_{τ} is essentially the same up until $r_{\perp} \simeq 2 \text{ pMpc}$. Therefore the density profile of halos mainly causes the decline of dN/dz at low r_{\perp} seen up to $\sim 1 \text{ pMpc}$.

At higher r_{\perp} ($> 3 \text{ pMpc}$ for Illustris and $> 1 \text{ pMpc}$ for IllustrisTNG) the median T_{τ} starts to drop with increasing r_{\perp} which compensates the decreasing Δ_{τ} (see Fig. 10). Depending of the rate of change of T_{τ} and Δ_{τ} with r_{\perp} either the $dN/dz(r_{\perp})$ flattens, as in the case of IllustrisTNG ($1 < r_{\perp} < 5 \text{ pMpc}$; Fig. 9) or $dN/dz(r_{\perp})$ increases as in the case of IllustrisTNG ($2 < r_{\perp} < 10 \text{ pMpc}$; Fig. 9).

At very high impact parameters ($r_{\perp} > 20 \text{ pMpc}$) median T_{τ} and Δ_{τ} remains constant with r_{\perp} (Fig. 10) as they converge to T_{τ} and Δ_{τ} for the IGM. This results in a constant $dN/dz(r_{\perp})$ for both simulations. Also the values of this asymptotic dN/dz for IGM is shown by dotted lines in Fig. 9 to which $dN/dz(r_{\perp})$ from both simulations converge at high $r_{\perp} > 20 \text{ pMpc}$.

Interestingly, in the case of Illustris the dN/dz goes below the dN/dz of IGM for a range of intermediate impact parameters $0.7 < r_{\perp} < 3 \text{ pMpc}$. This is mainly because Illustris expels a huge amount of gas from the CGM of galaxies into the IGM. This is why the median Δ_{τ} (see Fig 10) for Illustris is lower than the IllustrisTNG (by an order of magnitude) near halos ($r_{\perp} < 1 \text{ pMpc}$) and higher than IllustrisTNG at large impact parameters ($r_{\perp} > 1 \text{ pMpc}$). The constant offset between Δ_{τ} at higher impact parameters ($r_{\perp} > 10 \text{ pMpc}$) arises because of higher T_{τ} in Illustris requiring the higher over-densities to produce the $\text{Ly}\alpha$ absorption. The mean flux shown in (right-hand panel of) Fig. 10 shows that the mean flux for Illustris rises beyond the mean flux of the IGM at intermediate r_{\perp} ($0.8 < r_{\perp} < 20 \text{ pMpc}$) providing lower than IGM dN/dz (see Fig. 9) and then it drops to give a rise in dN/dz as seen in Fig. 9. However, even though asymptotic values of T_{τ} and Δ_{τ} at largest impact parameters in both simulations are different, mean $\text{Ly}\alpha$ flux in both simulations converge to the mean flux of the IGM (right-hand panel of Fig. 10) because of our calibrated Γ_{HI} .

As shown in Fig. 9, Illustris and IllustrisTNG simulations provide very different $dN/dz(r_{\perp})$ profile around massive halos. Up to an impact parameter of 5 pMpc i.e. $\sim 10R_{\text{vir}}$, the $dN/dz(r_{\perp})$ obtained for IllustrisTNG is a factor of $1.5 - 2$ times higher than the one obtained for Illustris. This is the consequence of the different feedback prescriptions employed in the simulations. The difference in $dN/dz(r_{\perp})$ can be seen until $r_{\perp} \sim 20 \text{ pMpc}$ ($\sim 40R_{\text{vir}}$). This striking difference in the $dN/dz(r_{\perp})$ suggests that it will be a powerful tool to study the impact of AGN feedback. Moreover, the observed $dN/dz(r_{\perp})$ determined from HST-COS data at low- z can be a benchmark observation against which simulations can test and calibrate their feedback models. Motivated by this, in what follows we perform a feasibility analysis to investigate if the currently available HST-COS quasar spectra probing massive halos hosting LRGs have constraining power to distinguish feedback models in Illustris and IllustrisTNG.

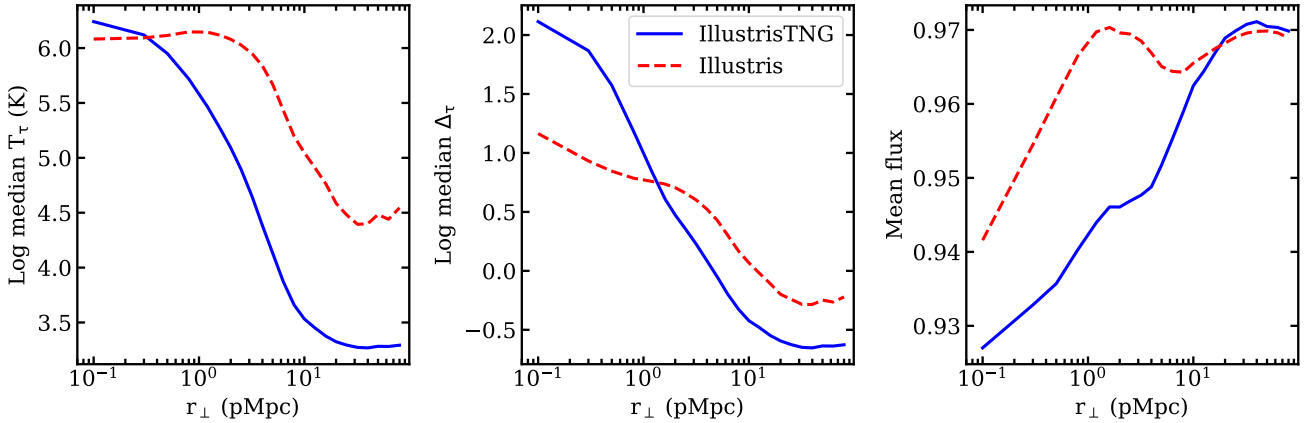


Figure 10. Median of optical depth weighted temperature T_τ (left-hand panel) and overdensity Δ_τ (middle panel), and mean Ly α flux (right-hand panel) for the line of sights passing at different impact parameters (r_\perp) along $\pm 500 \text{ km s}^{-1}$ of the position of halos for Illustris (dashed curves) and IllustrisTNG (solid curves). The differences in all three quantities help explaining the trend in $dN/dz(r_\perp)$ seen in Fig. 9 (as discussed in the Section 4.2).

4.3 The Feasibility of using the Line Density Profile as a Probe of the Feedback

We have performed forward models taking into account the S/N and redshift distribution of set of 94 HST-COS background quasar spectra that probe 3193 foreground LRGs (see Section 4.3 and Fig. 3). Therefore for the feasibility analysis, we use r_\perp distribution of LRGs (right-hand panel of Fig. 3) to estimate the precision one can obtain on the $dN/dz(r_\perp)$. For that, we re-bin the impact parameter distribution of these LRGs in logarithmic bins. We chose the bin centers such that they match the centers of our impact parameter bins where we have performed previous analyses in the simulations. We determine the number N^{bin} of LRGs in each impact parameter bin. With this information, for every impact parameter bin we randomly choose N^{bin} forward-modelled halo sightlines falling in the corresponding impact parameter bin of the simulations. By doing this at each impact parameter bin, we are choosing a forward model Ly α sightlines for each LRG-quasar pair passing within the respective (r_\perp) bin in simulations. We call this as our first random sample. We generate such 2000 random samples. We generate these samples only using IllustrisTNG simulation thereby assuming it to be the underlying true model. Since we have already run VPfit on forward modeled Ly α spectra, for each sample we determine the N_{HI} values within the same velocity window of $\pm 500 \text{ km s}^{-1}$ N_{HI} range and estimate the dN/dz for absorption lines and calculate the sample average of dN/dz and its variance.

We show these mock measurements i.e the sample average dN/dz and its variance, in Fig.9 by black data points with error bars. These mock measurements are the result of an ensemble of 2000 measurements. As expected the sample mean of dN/dz falls on the curve representing the true model i.e. the IllustrisTNG simulation. Since there are a large number of absorbers per bin we can find the statistical significance s of these mock measurement to distinguish dN/dz of IllustrisTNG (the true model) from Illustris using the following equation,

$$s^2 = \sum_i [\Delta(dN/dz)_i / \sigma_i]^2, \quad (1)$$

where i denotes i^{th} bin of impact parameter at which the mock measurements are done and the $\Delta(dN/dz)_i$ is the difference between the dN/dz of Illustris and our mock measurement in the same bin. We find that the mock dN/dz measurements can distinguish IllustrisTNG from Illustris simulation with a statistical significance of 12σ . Note that this is not actually the statistical significance of any given mock dataset but of an ensemble of datasets, since for a single dataset, there would be fluctuations.

This simple analysis reveals the potential of using the line density profile around halos $dN/dz(r_\perp)$ to constrain different feedback models used in galaxy formation simulations. Most of the feedback-constraining observations are related to the properties and distribution of galaxies whereas $dN/dz(r_\perp)$ uses the distribution of gas around galaxies up to 10 pMpc. Therefore, $dN/dz(r_\perp)$ holds considerable promise as it offers a complementary constraint for assessing the AGN feedback.

5 SUMMARY

Galaxy formation simulations rely on AGN feedback to regulate star formation in massive galaxies, a process involving powerful outflows and the heating of the surrounding gas in order to regulate star formation. However, these simulations cannot resolve the central AGNs directly, necessitating the use of sub-grid implementations for feedback modeling. While various feedback prescriptions are employed in simulations, their parameters are typically tuned based on observations, most of which pertain to galaxy properties and the immediate vicinity of galaxies within approximately the virial radius. What is lacking are benchmark observations that extend beyond galaxies, reaching into the IGM to probe and constrain these feedback models. This is a notable gap to address, given the relative ease of reproducing the IGM in simulations based on well-established theoretical foundations. Therefore, in this work, we seek summary statistics based on observations that are capable of probing the gas surrounding massive galaxies at vast distances with the potential to serve as a critical constraint for AGN feedback modeling.

To achieve this objective, we utilized two state-of-the-

art galaxy formation simulations; Illustris and IllustrisTNG at $z = 0.1$. These simulations are run with the same initial conditions and almost identical codes but with different feedback implementations. A notable difference is in the implementation of the radio mode AGN feedback which is very aggressive in the Illustris as compared to IllustrisTNG. As a result, the massive halos in the Illustris simulation generate large shock-heated regions surrounding them (see Fig. 1) extending up to 10 pMpc. Moreover, Illustris expels large amounts of gas from the halos of galaxies. It was in fact one of the key observations that prompted different AGN feedback prescriptions in the IllustrisTNG (see Weinberger et al. 2017; Pillepich et al. 2018a). As a result of different AGN feedback prescriptions, these two simulations are ideal for testing the effect of AGN feedback on the properties of gas around halos and in the IGM.

Because the fraction gas in the diffuse low-temperature gas that is responsible for the observed Ly α absorption is quite different in both simulations (23.2% in Illustris and 38.5% in IllustrisTNG), we perform a calibration of the UV background in each simulation. This calibration involves adjusting Γ_{HI} to ensure that both simulations yield the same observed Ly α line density dN/dz for the IGM. This calibration process, as outlined in Paper I, is essential to facilitate meaningful comparisons between the simulations and observational data.

After tuning the Γ_{HI} in both simulations we select the halos that are potential hosts of LRGs and generate perfect ($S/N = 100$ with resolution 4.1 km s^{-1}) and mock HST COS Ly α forest spectra ($S/N = 7$ per pixel of 6 km s^{-1} ; 12 per COS resolution element) at different impact parameters r_{\perp} . We fit these spectra using our automatic Voigt profile code and study statistics such as 2D $b-N_{\text{HI}}$ distributions, b distributions, N_{HI} distributions and dN/dz with (r_{\perp}).

For perfect Ly α forest spectra very close to the halos within $\sim 2r_{\text{vir}}$, the shape of 2D $b-N_{\text{HI}}$ distributions is similar in both simulations and differs at higher impact parameters. (see Fig. 5, 6, 7 & A1). Lines move towards low b values and higher N_{HI} with increasing r_{\perp} . At very high impact parameters ($r_{\perp} > 10 \text{ pMpc}$) $b-N_{\text{HI}}$ distributions slowly converge to the $b-N_{\text{HI}}$ distributions of the IGM. But in forward modeled Ly α forest, the differences in the shape of $b-N_{\text{HI}}$ distributions diminish at all impact parameters. However, there is a clear difference in the normalization of 2D $b-N_{\text{HI}}$ distributions, which is proportional to the number of Ly α lines (see Fig. 8, A3 & A4). Motivated by this we calculate the $dN/dz(r_{\perp})$, i.e. Ly α line density profile, around halos for both Illustris and IllustrisTNG using forward modeled Ly α spectra. We find that $dN/dz(r_{\perp})$ obtained for IllustrisTNG is larger than Illustris by a factor of 1.5 – 2 up to an impact parameter of 10 pMpc (~ 20 viral radii; Fig 9). This significant difference in $dN/dz(r_{\perp})$ underscores its promising utility for probing and constraining diverse feedback implementations used in simulations

Lastly, we perform feasibility analysis using available archival data. We find that there are 3193 foreground LRGs probed by high-quality 94 HST COS background quasar spectra up to an impact parameter of 10 pMpc (see Fig. 3). Using their real impact parameter distribution and median S/N of the sample, we estimate precision on the mock $dN/dz(r_{\perp})$ measurement (see Fig. 9). We find that these mock measurements can differentiate between Illustris and IllustrisTNG

simulations with a statistical significance of 12σ . This demonstrates that the $dN/dz(r_{\perp})$ measurement around massive halos, derived from the presently available HST-COS data, holds the capacity to discern between extreme feedback models. Moreover, $dN/dz(r_{\perp})$ can serve as a valuable benchmark observation for rigorously testing and calibrating various feedback prescriptions employed in simulations.

ACKNOWLEDGEMENT

VK thanks D. Sorini and D. Nelson for helping with Illustris simulation datasets. VK thanks R. Srianand for hosting him at the Inter-University Centre for Astronomy and Astrophysics (IUCAA), Pune, India, and for helpful discussions on the paper. VK is supported through the INSPIRE Faculty Award (No.DST/INSPIRE/04/2019/001580) of the Department of Science and Technology (DST), India.

DATA AVAILABILITY

We utilized a subset of quasar spectra from the dataset presented in Danforth et al. (2016) which is accessible at <https://archive.stsci.edu/prepds/igm>. The simulation data is obtained from the Illustris website, with links provided in the text at relevant locations.

REFERENCES

- Berg M. A., et al., 2019, *ApJ*, **883**, 5
 Bolton J. S., Puchwein E., Sijacki D., Haehnelt M. G., Kim T.-S., Meiksin A., Regan J. A., Viel M., 2017, *MNRAS*, **464**, 897
 Burkhart B., Tillman M., Gurvich A. B., Bird S., Tonnesen S., Bryan G. L., Hernquist L., Somerville R. S., 2022, *ApJ*, **933**, L46
 Carswell R. F., Webb J. K., 2014, VPFIT: Voigt profile fitting program (ascl:1408.015)
 Chen H.-W., Zahedy F. S., Johnson S. D., Pierce R. M., Huang Y.-H., Weiner B. J., Gauthier J.-R., 2018, *MNRAS*, **479**, 2547
 Chen H.-W., et al., 2019, *MNRAS*, **484**, 431
 Croton D. J., et al., 2006, *MNRAS*, **365**, 11
 Danforth C. W., et al., 2016, *ApJ*, **817**, 111
 Davé R., Anglés-Alcázar D., Narayanan D., Li Q., Rafieferantsoa M. H., Appleby S., 2019, *MNRAS*, **486**, 2827
 Dubois Y., et al., 2014, *MNRAS*, **444**, 1453
 Faucher-Giguère C.-A., 2020, *MNRAS*, **493**, 1614
 Faucher-Giguère C.-A., Lidz A., Zaldarriaga M., Hernquist L., 2009, *ApJ*, **703**, 1416
 Genel S., et al., 2014a, *MNRAS*, **445**, 175
 Genel S., et al., 2014b, *MNRAS*, **445**, 175
 Guo H., et al., 2015, *MNRAS*, **453**, 4368
 Gurvich A., Burkhart B., Bird S., 2017, *ApJ*, **835**, 175
 Haardt F., Madau P., 2012, *ApJ*, **746**, 125
 Hiss H., Walther M., Hennawi J. F., Oñorbe J., O’Meara J. M., Rorai A., Lukić Z., 2018, *ApJ*, **865**, 42
 Hopkins P. F., Hernquist L., Cox T. J., Kereš D., 2008, *ApJS*, **175**, 356
 Hu T., et al., 2022, *MNRAS*, **515**, 2188
 Hu T., Khaira V., Hennawi J. F., Onorbe J., Walther M., Lukic Z., Davies F., 2023, *arXiv e-prints*, p. arXiv:2308.14738
 Khaira V., 2017, *MNRAS*, **471**, 255
 Khaira V., Srianand R., 2019, *MNRAS*, **484**, 4174
 Khaira V., et al., 2019, *MNRAS*, **486**, 769

- Khaire V., Hu T., Hennawi J. F., Walther M., Davies F., 2023, [arXiv e-prints](#), p. [arXiv:2306.05466](#)
- Khandai N., Di Matteo T., Croft R., Wilkins S., Feng Y., Tucker E., DeGraf C., Liu M.-S., 2015, *MNRAS*, **450**, 1349
- Lukić Z., Stark C. W., Nugent P., White M., Meiksin A. A., Almgren A., 2015, *MNRAS*, **446**, 3697
- Mallik S., Srianand R., Maitra S., Gaikwad P., Khandai N., 2023, *MNRAS*, **523**, 2296
- Naab T., Ostriker J. P., 2017, *ARA&A*, **55**, 59
- Naiman J. P., et al., 2018, *MNRAS*, **477**, 1206
- Nelson D., et al., 2018, *MNRAS*, **475**, 624
- Nelson D., et al., 2019, *MNRAS*, **490**, 3234
- Peeples M., et al., 2017, Technical report, The Hubble Spectroscopic Legacy Archive
- Pillepich A., et al., 2018a, *MNRAS*, **473**, 4077
- Pillepich A., et al., 2018b, *MNRAS*, **475**, 648
- Pillepich A., et al., 2019, *MNRAS*, **490**, 3196
- Rahmati A., Pawlik A. H., Raicevic M., Schaye J., 2013, *MNRAS*, **430**, 2427
- Schaye J., et al., 2015, *MNRAS*, **446**, 521
- Shull J. M., France K., Danforth C. W., Smith B., Tumlinson J., 2010, *ApJ*, **722**, 1312
- Sijacki D., Springel V., Di Matteo T., Hernquist L., 2007, *MNRAS*, **380**, 877
- Springel V., 2005, *MNRAS*, **364**, 1105
- Springel V., 2010, *MNRAS*, **401**, 791
- Tepper-García T., 2006, *MNRAS*, **369**, 2025
- Tillman M. T., Burkhart B., Tonnesen S., Bird S., Bryan G. L., Anglés-Alcázar D., Davé R., Genel S., 2022, [arXiv e-prints](#), p. [arXiv:2210.02467](#)
- Tojeiro R., et al., 2012, *MNRAS*, **424**, 136
- Vogelsberger M., et al., 2014, *MNRAS*, **444**, 1518
- Vogelsberger M., Marinacci F., Torrey P., Puchwein E., 2020, *Nature Reviews Physics*, **2**, 42
- Weinberger R., et al., 2017, *MNRAS*, **465**, 3291
- Werk J. K., Prochaska J. X., Thom C., Tumlinson J., Tripp T. M., O’Meara J. M., Meiring J. D., 2012, *ApJS*, **198**, 3
- Worseck G., et al., 2011, *ApJ*, **733**, L24
- York D. G., et al., 2000, *AJ*, **120**, 1579
- Zahedy F. S., Chen H.-W., Johnson S. D., Pierce R. M., Rauch M., Huang Y.-H., Weiner B. J., Gauthier J.-R., 2019, *MNRAS*, **484**, 2257
- Zehavi I., et al., 2011, *ApJ*, **736**, 59

APPENDIX A: THE 2D AND MARGINALIZED DISTRIBUTION OF DOPPLER PARAMETER AND N_{HI} AROUND HALOS

In this section, we show additional figures of 2D and marginalized b - N_{HI} distributions at other impact parameter bins than the one shown in Fig. 5, 6, 7 & 8. The KDE estimated 2D b - N_{HI} distributions are shown in Fig. A1 and A2 and histograms of b (left-hand panels) and N_{HI} (right-hand panels) for forward modeled sightlines are shown in Fig. A3 and A4. See Section 4.1 for the discussion.

This paper has been typeset from a $\text{\TeX}/\text{\LaTeX}$ file prepared by the author.

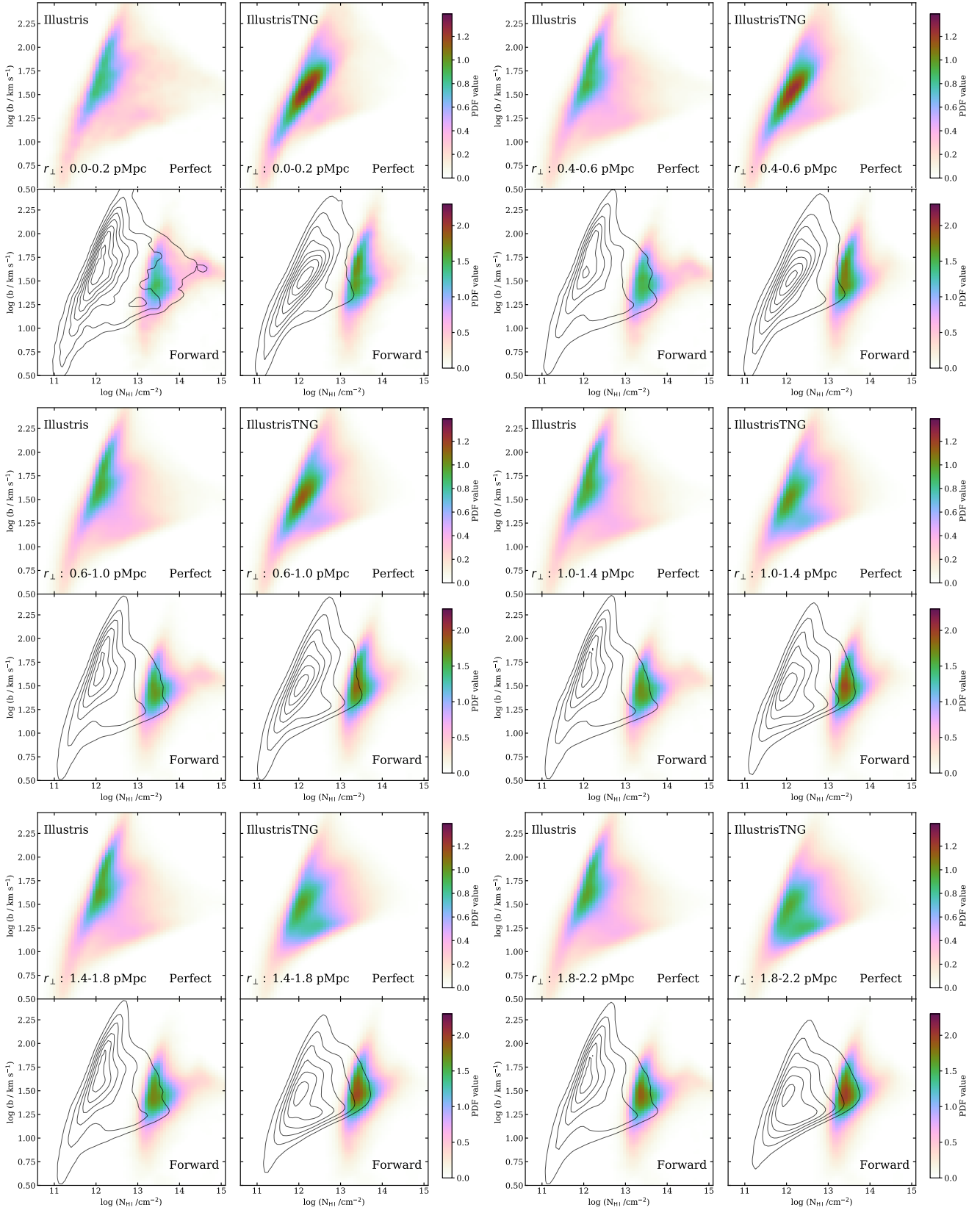


Figure A1. Same as Fig. 5, the 2D b - N_{HI} distribution around massive halos at six different impact parameters (indicated in legends) from 0 to 2.2 pMpc. With increasing impact parameters the shape and normalization (indicated by color) of the distribution evolves.

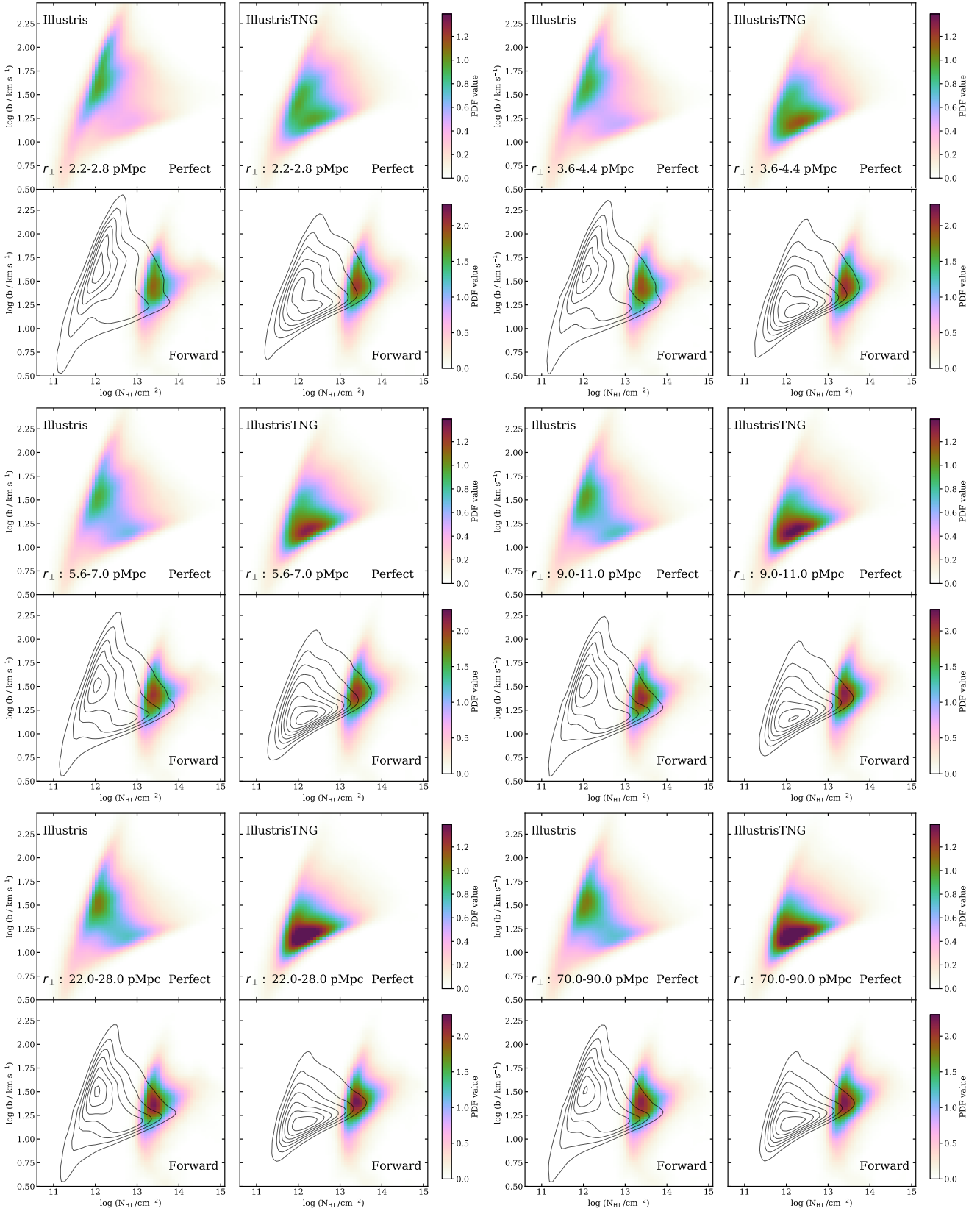


Figure A2. Same as Fig. 5, the 2D b - $N_{\text{H I}}$ distribution around massive halos at six different impact parameters (indicated in legends) from 2.2 to 90 pMpc. With increasing impact parameters, the shape of the distribution evolves and converges to the one obtained for the IGM (see Paper I).

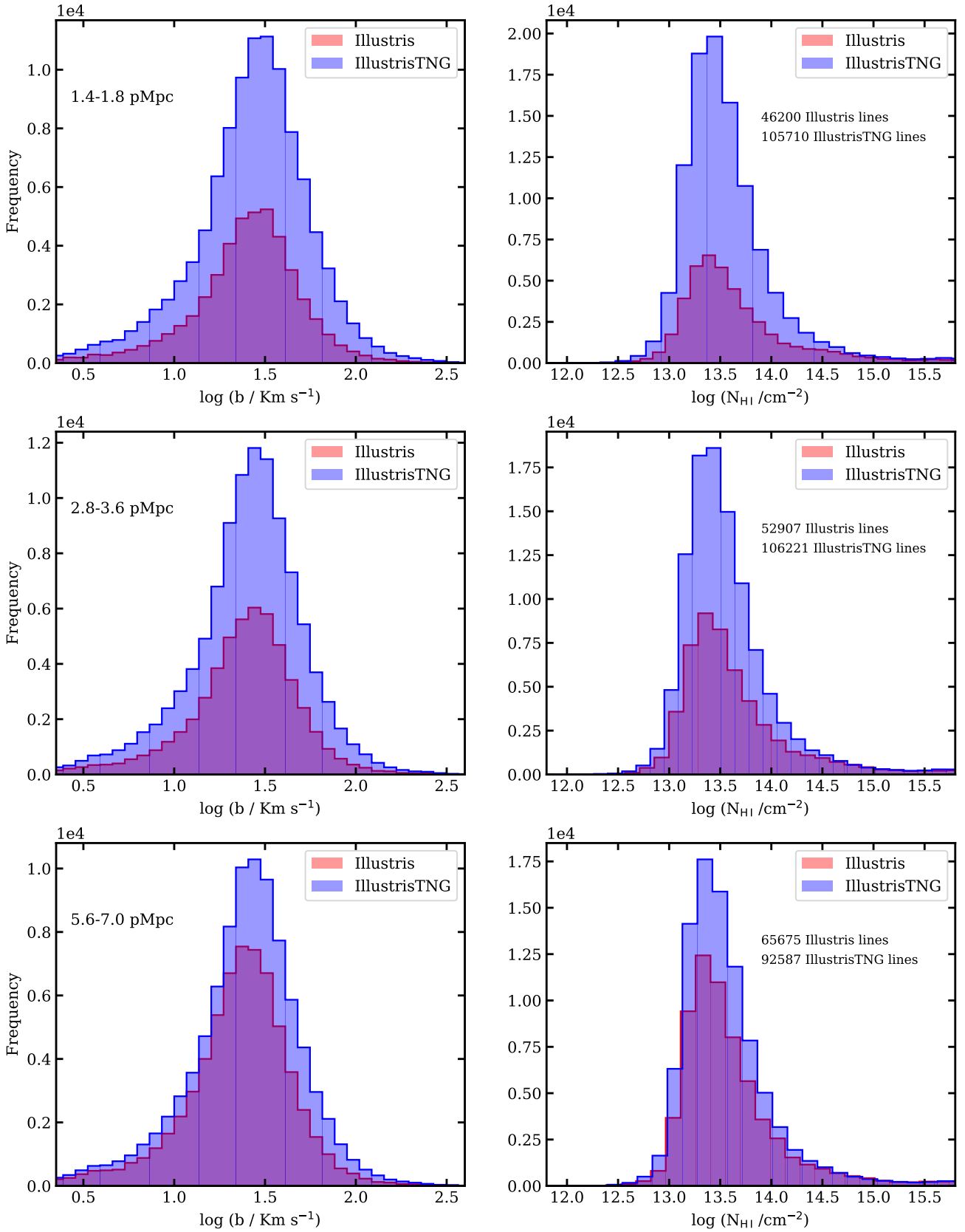


Figure A3. The b (right) and N_{HI} (left) distribution from the forward-modeled sightlines generated at different impact parameter bins (see legends - left panel) for Illustris and IllustrisTNG. The number of lines in each histogram is given in the legend (right-panels).

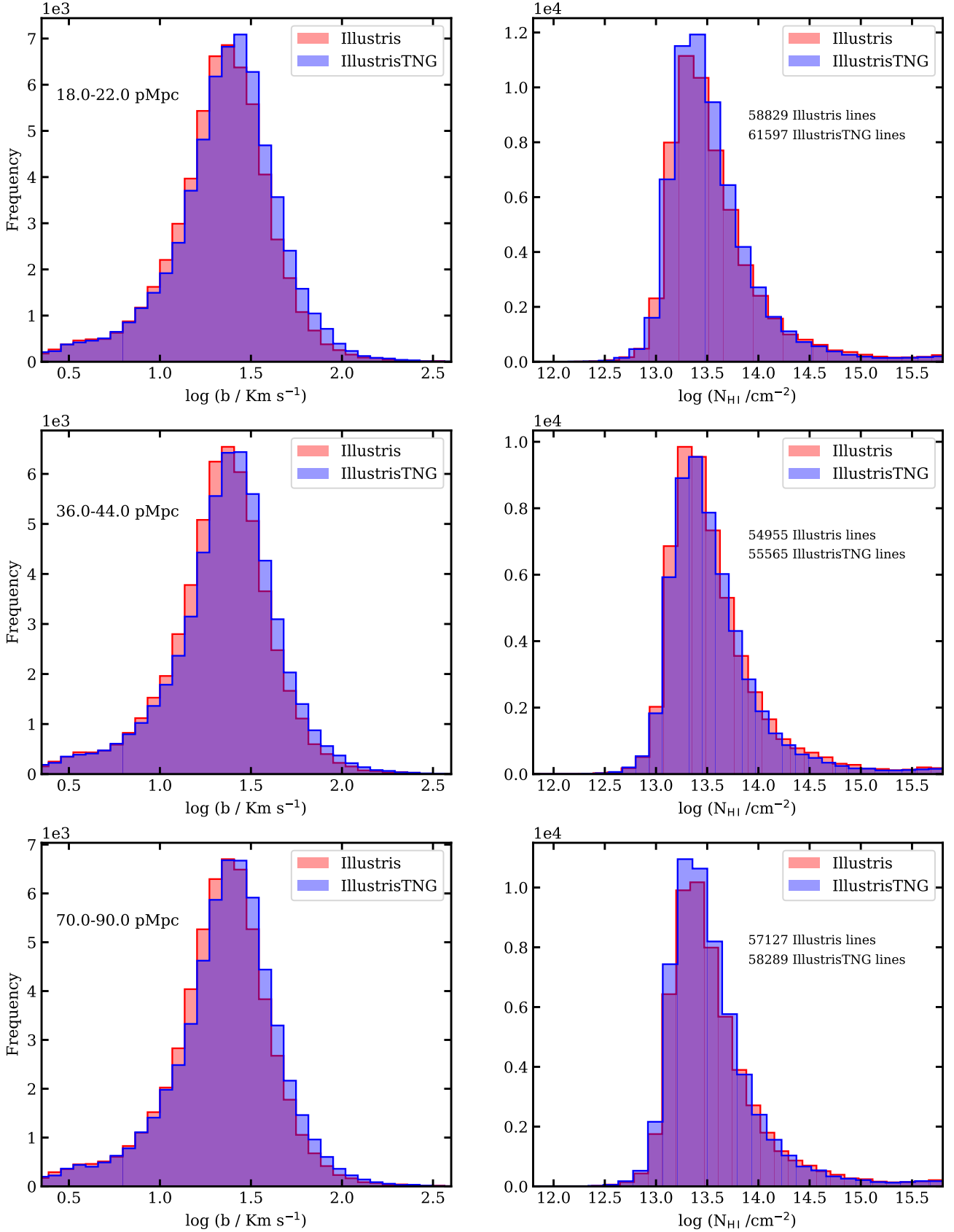


Figure A4. Same as Fig. A3 but for different impact parameters. The number of lines match closely (within $\sim 2\%$) for both simulations at high impacts converging to the values for the IGM.